Chapter 4-Advanced Acoustic Modeling

Chapter 3 provided the background information needed to model the single injector test rig and also showed that a 1-D acoustic transmission line approach could capture the important dynamics of the test rig. Following the same approach as before, individual components will be modeled and then assembled, forming an entire test rig acoustic model. This approach is limited by the fact that not all of the components of the test rig can be tested individually. Component modeling will focus on the combustion liner and the injector which are the most important parts of the test rig. Once the complete single injector test rig model has been refined, the acoustics can be scaled to the operating temperature and pressure to provide the acoustic transfer function needed for the linear stability analysis.

4.1-Combustion Liner Modeling

Two major types of combustion liners are used in the single injector test rig. Figures 4.1a and 4.1b show schematics of a louver liner and a backside cooled liner respectively. Because the flame resides in the liner, it must be designed to handle extremely high temperatures. The difference between the louver and backside cooled liner is in how the liner walls are cooled. The louver liner relies on perforates around the circumference and internal louvers to create film cooling along the wall. The backside cooled liner has a narrow annulus jacketing the liner in which high velocity air increases the amount of convective heat transfer on the outside of the liner wall. This air then dilutes the exhaust flow of the combustor through the four large dilution holes shown in Figure 4.1b. The acoustic modeling of these components will focus on how to model the perforated wall of the louver liner and the narrow annulus of the backside cooled liner.

The models created for these liners will be compared to data taken at Solar Turbines Incorporated. During the test rig experiments the liners were removed from the test rig and tested as individual components. The test arrangement included blocking the injector inlet with a ¾” piece of plywood while the outlet radiated into the open air. The liners were excited by hanging a speaker near the assumed location of the flame. Their acoustic response was captured by two microphones placed approximately 4” downstream of the speaker and at the open end of the liner.

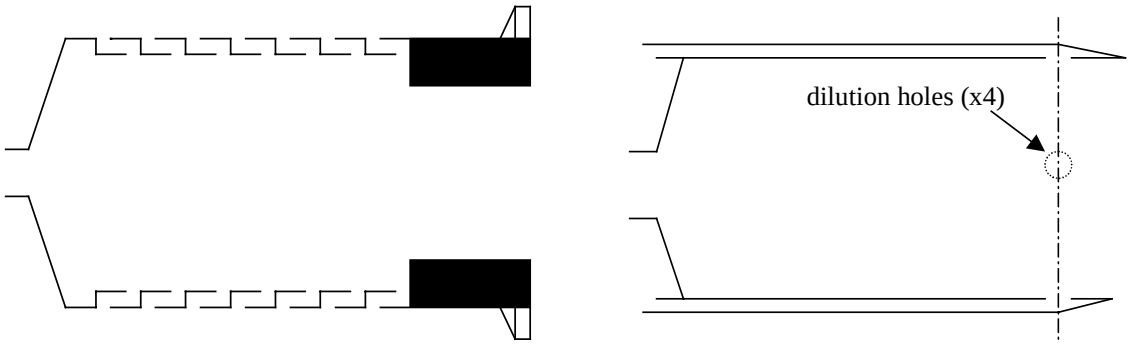

Louver Liner (a) **Backside Cooled Liner (b)**

Figure 4.1 a,b-Schematics of louver liner and backside cooled liner.

4.1.1-Louver Liner Modeling

The experiments performed on the louver liner may seem like a deviation from the actual configuration of the liner in the test rig because it actuality does not radiate to the open air. However, the blocked-inlet experimental configuration was the only way to determine the best type of model for the perforates without dealing with the extra complications of the entire rig. Figure 4.2 shows the initial approach to modeling the louver liner. Section 3.3.3 explains how to model the parallel path at the speaker plane. The parallel path is also used to account for the perforates in the liner walls. In Figure 4.2, there is an element of some thickness and diameter at each of the cross-sectional planes where the liner is perforated. At this boundary the pressure must remain continuous and the volume velocity into the boundary must equal the sum of the volume velocity leaving the boundary and the volume velocity through the perforated holes. The holes in a plane around the liner's circumference are modeled as a single element of area equal to the summation of all the individual hole areas. A radiation impedance which must be determined is used as the boundary condition outside the liner.

At first glance it may seem that an acoustic pressure equal to zero should be used as the external boundary condition for a perforate since atmospheric pressure surrounds the liner, but this is not the case. Because the hole radiates energy to the surroundings there exists an acoustic pressure outside the hole which is not zero, and therefore the hole must be modeled with some impedance. This impedance is equivalent to the radiation of a piston at the hole's boundary. Equation 4.1a shows the exact radiation impedance, where $J_1(x)$ is a Bessel function of order 1, and $H_1(x)$ is a Struve function of order 1. If

ka<<1 then a low-frequency approximation can be obtained by taking the first term in the power series representation of each function, as shown in Equation 4.1b.

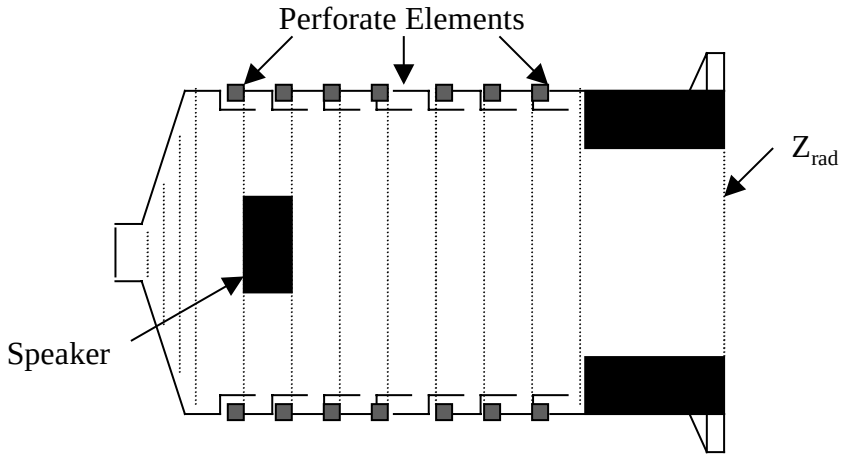

Figure 4.2-Schematic of louver liner with initial boundary conditions.

$$Z_{rad} = \frac{f}{u} = \rho_0 cS[R_1(2ka) + jX_1(2ka)]$$
$$R_1(x) = 1 - \frac{2J_1(x)}{x}; X_1(x) = \frac{2H_1(x)}{x} \quad (4.1a)$$

$$R_r \approx \frac{1}{2}\rho_0 cS(ka)^2; X_r \approx \frac{8}{3\pi}\rho_0 cS(ka) \quad (4.1b)$$

The radiation impedance is also used as the boundary condition at the open end of the combustion liner. Because ka≈1 for the open end, the low-frequency approximation can not be used. However, no closed-form solution exists for either the Bessel or Struve function since they are both infinite power series. It was determined that a three term expansion of the radiation resistance (R_r) and reactance (X_r) was accurate enough for the radius and frequency bandwidth in question. Equation 4.2 shows how this boundary condition is implemented into the coefficient matrix equation **Ax**=**b**. The unknown amplitudes (A_n and B_n) of the n^{th} element go in the **x** vector, 0 goes in forcing vector **b**, and the rest of the terms go in the **A** matrix with the exponential terms evaluated at the location of the boundary.

$$A_n(\rho cS - Z_{rad})e^{-jkx} + B_n(\rho cS + Z_{rad})e^{jkx} = 0 \quad (4.2)$$

With the boundary conditions defined for all elements, a model can be constructed simply by connecting each element with the appropriate boundary conditions and constructing the coefficient matrix equation as described in Section 3.1. Using the modeling approach discussed above, 21 elements (42 unknown amplitudes) are needed to model the louver liner. Figure 4.3 shows the FRF of the initial model created for the louver liner. The high frequency mode matches with the data, but the low frequency mode is off by 50 Hz, and it does not have the proper damping. After numerous refinements, the model still failed to match the experimental data. The perforates and the radiation impedance were the only two components of the louver liner which had not been validated by the tube modeling, therefore it was decided to build a closed-open tube with geometrical features similar to the combustion liner. With the new model, individual components could be isolated for investigation.

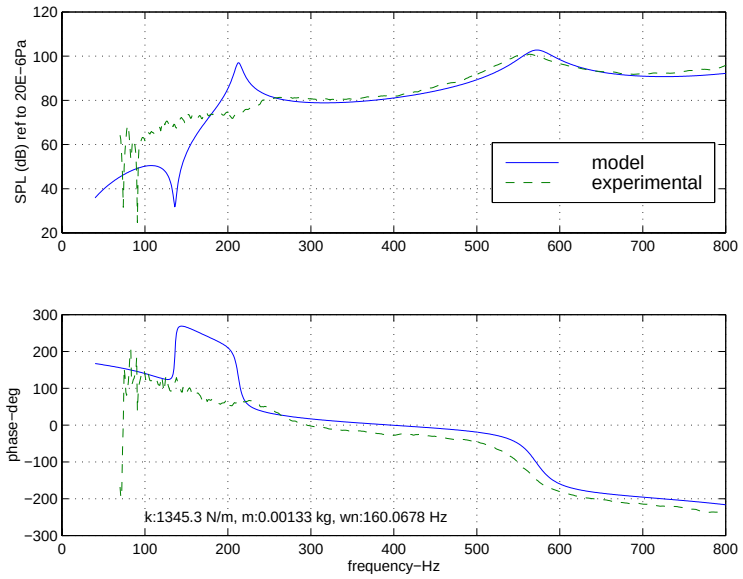

Figure 4.3-FRF of louver liner with perforates modeled as wave elements.

4.1.2-Closed-Open Tube Modeling

The goal in returning to modeling tubes was to isolate individual components and make sure each one could be accurately modeled. The first model would be a closed-open tube driven internally in which one would nominally expect quarter-waves to form. A plug would then be added to match the area ratio of the plug in the louver liner. Finally, rows of holes would be added around the circumference of the tube to account for the perforates in the louver liner. The first model can easily be constructed with only two boundary conditions. The rigid wall has zero particle velocity (u(x=0)=0), and the open end has a radiation impedance given by Equation 4.1a. Figure 4.4 shows the FRF of a simple closed-open tube model and, as would be expected, the resonant frequencies occur near λ/4, 3λ/4, 5λ/4…. Based on a tube length of 36" the respective frequencies are 93 Hz, 281 Hz, and 468 Hz. These theoretical frequencies are slightly different from the frequencies seen in Figure 4.4 due to the radiation impedance at the open end of the liner. Using this simple model, the radiation impedance value for the open end was validated, allowing another degree of complexity to be added to the tube model.

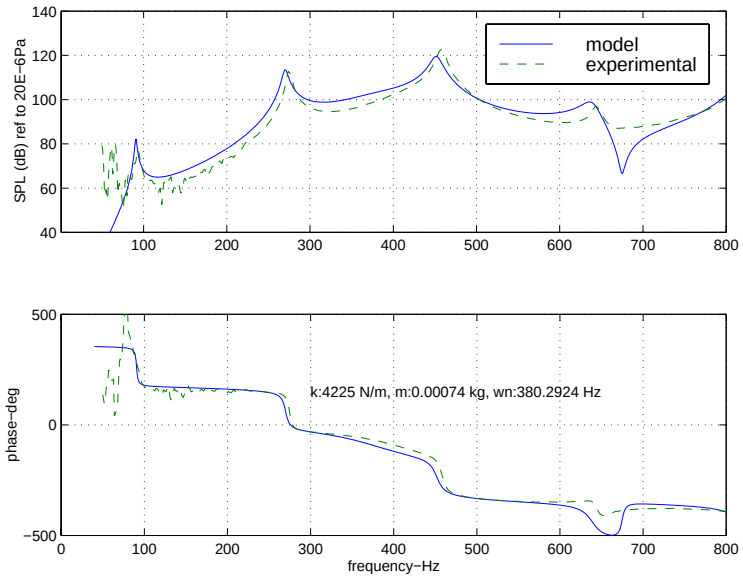

Figure 4.4-FRF of closed-open tube driven internally.

A plug was the next degree of complexity added to the tube. In order to create a tube model more geometrically proportional to the louver liner the 36" length

tube was reduced to 7.5” so that the l/d ratio would be similar to that of the louver liner. A plug of l=1.5” and d=2.75” was then inserted into the open end of the tube to mimic the ceramic plug used in the louver liner. Modeling the plug is a very simple matter of adding an additional element which acts as an area restriction. Figure 4.5 is an FRF of the 7.5” long closed-open tube with a 2.75” diameter plug. Given the boundary conditions, the resonant frequencies might be expected at 450 Hz and 1350 Hz, but instead the FRF response has peaks at 315 Hz and 1145 Hz. Thus, the plug has a “mass” like effect on the system by lowering the acoustic resonant frequencies. Again, the gradual negative slope of the phase represents the speaker phase superimposed on the acoustic response.

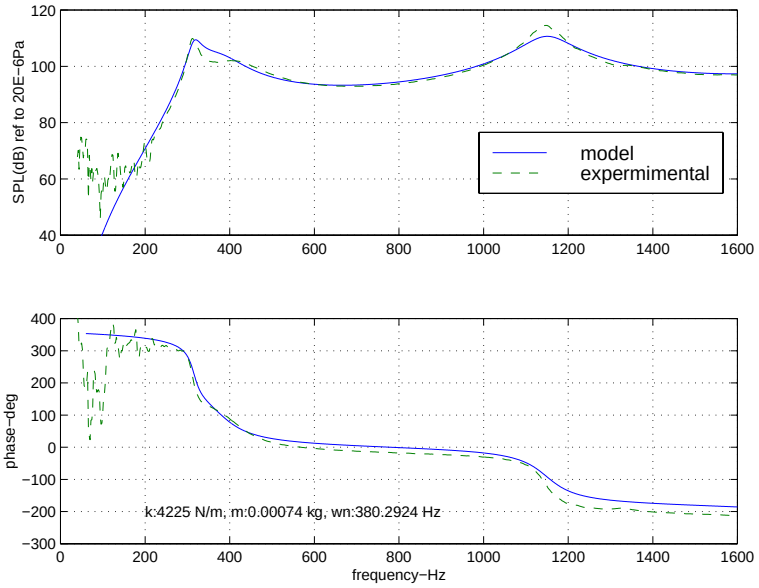

Figure 4.5-FRF of closed-open tube driven internally with plug.

The last degree of complexity added to the tube model was holes around the circumference. As with the initial attempts at modeling the louver liner, using elements with an external radiation impedance failed to produce the correct FRF. The next approach treated the small holes as bulk elements. The type of bulk element used is known as a continuous volume velocity two-port and is valid to use at low frequency and short lengths where the phase change across the element is negligible. Since a continuous volume velocity two-port does not correspond to waves in each hole, its only function is to change the impedance inside the liner at the plane where the holes exist. To

incorporate the bulk elements into the overall model, a junction impedance is needed. Equation 4.4 shows the theoretical junction impedance provided by Pierce [24] for an orifice in a thin plate. This impedance is entirely reactive (imaginary) and, if *l* is considered to be negligible, the junction impedance looks very similar to the low frequency approximation used for the reactive part of the radiation impedance shown in Equation 4.1b.

$$Z_{junct} = -j\omega M_A, M_A = \frac{\rho l}{\pi a^2} + \frac{\rho}{2a} \quad (4.3)$$

Using the junction impedance, the boundary conditions at each plane can be specified by Equation 4.4. As stated previously, the pressure must be continuous across the boundary and the sum of the volume velocities entering the boundary must equal the sum of the volume velocities leaving the boundary. The other issue which must be addressed is how to deal with not just one hole, but numerous holes in the same plane. Using an effective area based on all the holes would yield misleading results since the junction impedance would be calculated on a radius (*a*) much larger than each individual hole. A more reasonable approach is to multiply a single hole's volume velocity by the total number of holes (*n*), which is shown in Equation 4.4. An advantage to using bulk elements is that they reduce the number of amplitude coefficients which must be found, thus lowering the computational cost.

$$\begin{gathered} p_1(x = l_1) = p_2(x = 0) \\ V_1(x = l_1)S_1 = V_2(x = 0)S_2 + \frac{n(p_1(x = l_1) - p_0)}{Z_{junct}} \end{gathered} \quad (4.4)$$

Using the boundary conditions specified in Equation 4.4, a numerical model was created with holes in the tube walls. To maintain some relative scaling to the louver liner the number and size of the holes in the tube were proportional to the number and size of the holes in the louver liner. This resulted in six rows of holes with nineteen 0.0635" diameter holes per row. To see how the system's frequency response would be affected,

the holes were added one row at a time. Each additional row of holes changed the experimental FRF slightly, moving the low frequency peak higher while having little effect on the high frequency peak. As additional rows were added to the model it slowly lost its ability to follow the experimental data. Two issues were addressed in order to fix the model. First, since the junction impedance is entirely reactive, it does not allow for any energy loss, which obviously occurs through the holes to the outside environment. To account for this energy loss, a small resistive (real) part of approximately 25% of the reactive part was added to the junction impedance. This added damping to the peaks so that they fit the experimental data better. The second issue addressed the validity of using a junction impedance designed for a single hole to model a number of holes. Even though the number of holes was factored into the volume velocity equation it was thought that the value used for the junction impedance may need a corrective factor to account for the coupling of the fluid velocities of adjacent holes. Using a multiplication factor of 1.25 resulted in a model which matched very well with the experimental data obtained from the tube. Figure 4.6 shows how the holes change the system's response. As more rows of holes are added, the low frequency peak moves to a higher frequency, but the higher frequency peak changes very little. This can be explained by examining the value of the junction impedance as ω increases. In the limit as ω goes to infinity the holes look like rigid walls, therefore one expects the junction impedance to have very little affect at high frequency.

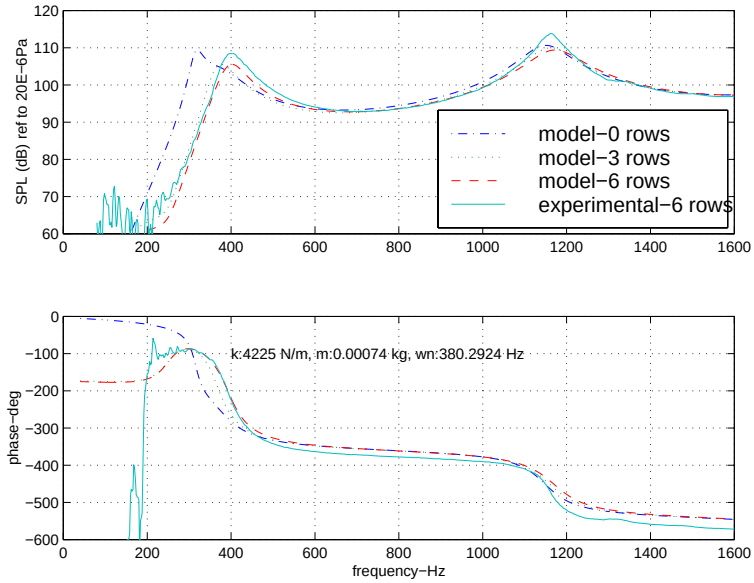

Figure 4.6-FRF of closed-open tube with plug showing influence of perforates.

4.1.3-Injector Modeling

Another important component of the sub-scale combustor test rig is the fuel injector where air and fuel are pre-mixed together and then swirled before being combusted. An injector obtained from Solar Turbines was placed into the plugged end of the perforated tube model created in the previous section in order to model its acoustics. Figure 4.7a shows a diagram of the fuel injector and a schematic of how the injector was broken into transmission line elements (Figure 4.7b). Element boundaries were chosen based on significant area changes in the injector. Initial attempts to model the injector were based on the assumption that the fuel system was choked and the center body did not participate in the response, thus the swirler vanes were the only part of the injector which had to be modeled. Because of the low frequency band considered, the acoustic waves are affected very little by the swirler geometry, so a simple area restriction will adequately model the swirler section.

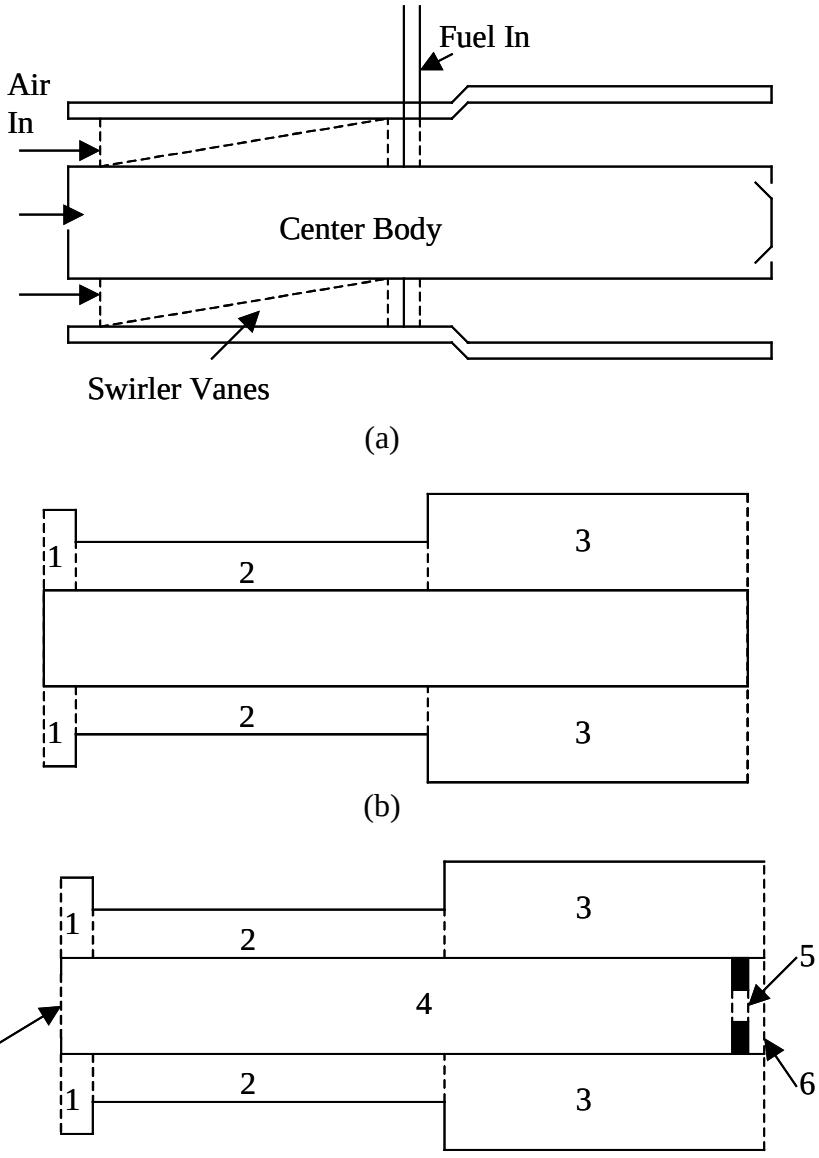

Figure 4.7 a,b,c-(a) Drawing of injector. (b) Basic acoustic element model. (c) Detailed acoustic element model.

Figure 4.8a shows the tube system FRF using the simplified injector model. In general, this response looks similar to the closed-open perforated tube discussed in the last section except for the large peak near 850 Hz. From this result it is obvious that some of the assumptions made about the injector are incorrect. In order to isolate the section of the injector which changed the system's response, experiments were conducted on each of its individual sections. Through this process it was found that the center body geometry contributed to the high frequency dynamics of the system. The center body geometry

was then added to the model, as shown in Figure 4.7c. Figure 4.8b shows the FRF of the injector model including the center body geometry. From this exercise it can be concluded that the simplified model does not capture all of the injector dynamics, but in the low frequency band (0-600 Hz) being considered in the modeling of the full rig, the simplified model provides adequate results.

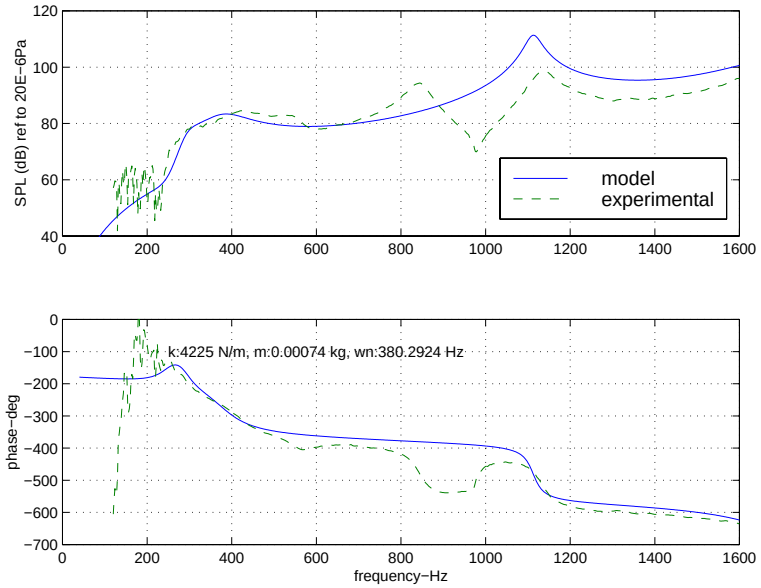

(a)

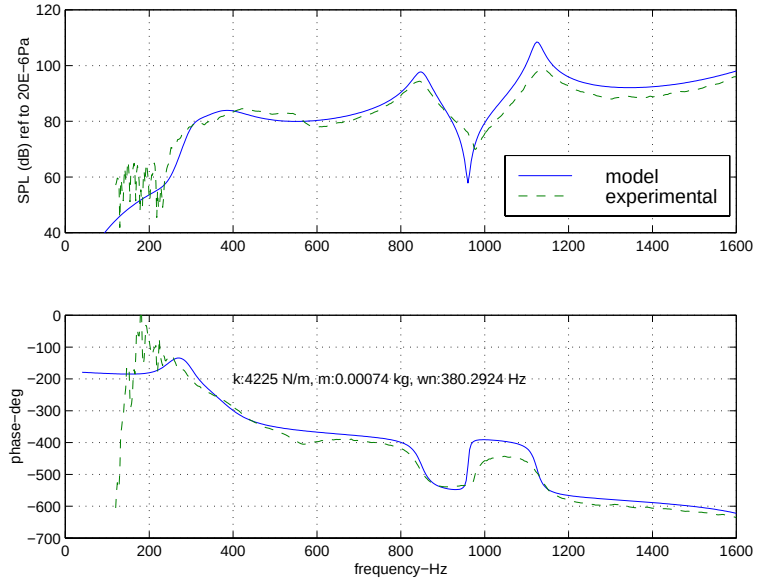

(b)

Figure 4.8 a,b-(a) FRF of simple injector model in closed-open tube. (b) FRF of detailed injector model in closed-open tube.

4.1.4-Louver Liner Modeling (Revisited)

Based on the knowledge gained from the perforated tube, the model for the louver liner was improved by using junction impedances for the perforates in the liner. The theoretical impedance values were adjusted until the model matched the experimental data. The impedance corrections which resulted in the best matching occurred using a multiplication factor of 1.5 times the theoretical value, and a resistive (real) component equal to between 25-35% of the reactive (imaginary) part. The simplest case to examine is the louver liner without a refractory plug. This liner has ten rows of louvers with ninety holes per row. The hole diameters are .05" for the first five rows, and .032" for the last five rows. Figure 4.9 is an FRF of the louver liner without a refractory plug. It can be seen that the perforates have a profound affect on the frequency of the 1st acoustic mode, raising it almost 100 Hz above the expected quarter-wave frequency for a 17.8" length closed-open tube. It should be noted that the data shown in Figures 4.9 and 4.10 was obtained from experimental liner tests conducted at Virginia Tech after errors were found in the data taken for the louver liner at Solar Turbines.

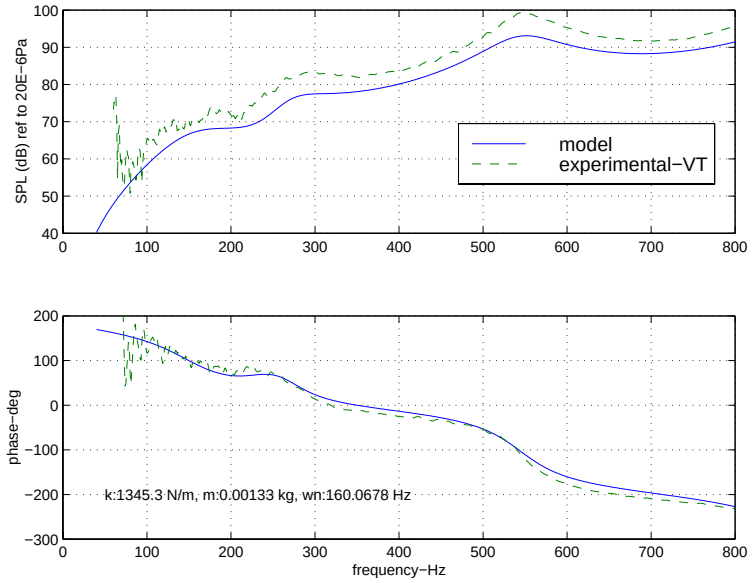

Figure 4.9-FRF of louver liner w/o plug using a junction impedance for the perforates.

Figure 4.10 shows the system response of the louver liner with the 5.75" diameter plug. Comparing this FRF with Figure 4.3 one can see that the junction impedance approach corrected both the 1st acoustic mode's resonant frequency and damping, while having very little impact on the 2nd acoustic mode. The junction impedance had a similar affect on the perforated tube as explained at the end of Section 4.1.2. Comparing the louver liner with and without a plug (Figure 4.10 and Figure 4.9, respectively), reveals that the plug lowers the natural frequency of the 1st acoustic mode, but has little affect on the frequency of the 2nd acoustic mode. Two reasons account for this behavior. First, when the plug is inserted, the number of rows of holes is reduced from ten to seven. The tube experiments showed that additional rows increased the 1st mode's natural frequency, therefore lowering the number of rows would tend to lower the natural frequency. Secondly, as shown by Figure 3.14b, a factor of two area reduction with a length ratio of approximately 0.4 lowers the 1st mode's frequency, while having little effect on the frequency of the 2nd mode. It should be noted that this is not a direct comparison since Figure 3.14b does not contain perforates, but rather it provides a qualitative explanation for the changes seen in the system response.

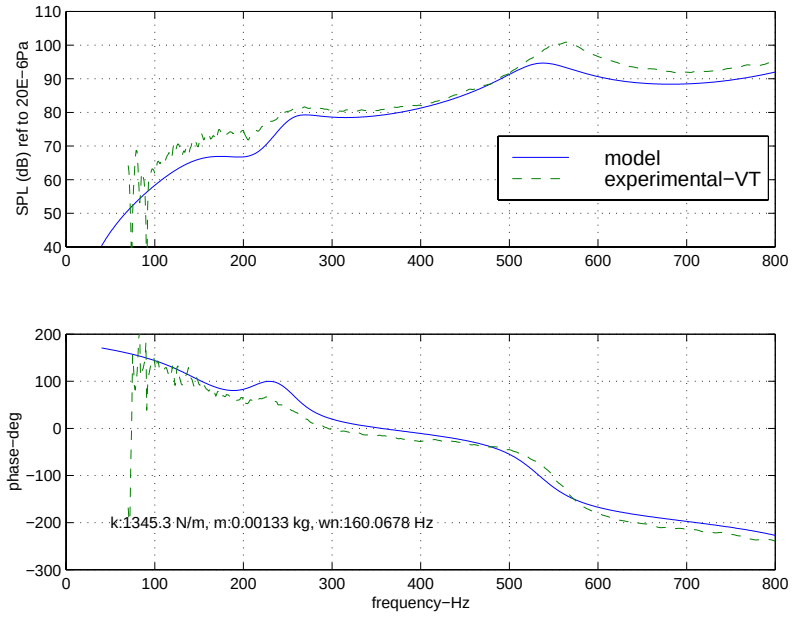

Figure 4.10-FRF of louver liner w/ plug using a junction impedance for the perforates.

4.1.5-Backside Cooled Liner Modeling

Figure 4.1 shows a schematic of the backside cooled (BSC) liner. This model is actually simpler than the louver liner since the liner walls are rigid. The only complications with the BSC liner are modeling the four dilution holes near the liner exit and the annular radiation impedance at the inlet of the narrow annulus jacket. These items are part of the element layout shown in Figure 4.11. A satisfactory model for the annular radiation impedance is found by applying the standard radiation impedance to the effective area of the annulus section. The boundary condition for the dilution holes was much more difficult to obtain.

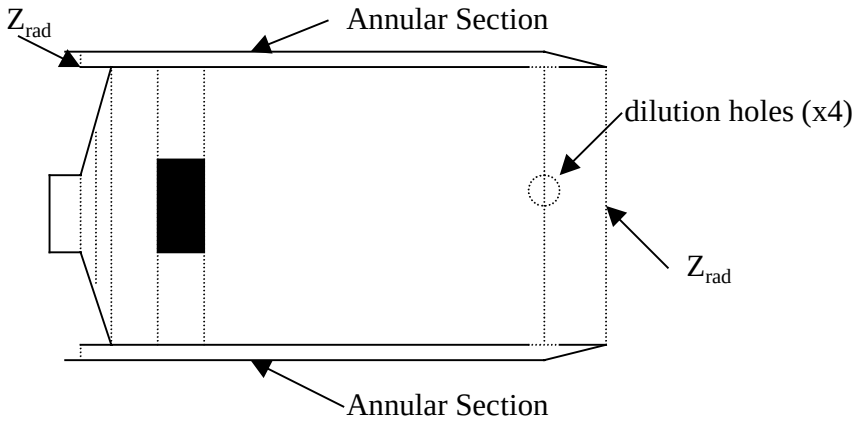

Figure 4.11-Backside cooled liner element model.

Since the junction impedance proved itself useful in the past, it was used as the first modeling approach for the dilution holes. Figure 4.12a shows the FRF of the BSC liner with the dilution holes modeled using a junction impedance. In general the model captures most of the relevant dynamics of the liner. As expected, the quarter-wave frequencies, for a closed-open configuration, of 190 Hz for $\lambda/4$ and 569 Hz for $3\lambda/4$ are predicted by the model. The model fails to capture a lower energy resonance seen in the data at 350 Hz. Because this resonance is so week in the main section of the liner it was thought to be from the annulus sub-section. A junction impedance allows the dynamics of one sub-section to impede the dynamics of the other sub-section at a point, but it will not allow waves in one sub-section to travel into another sub-section. Thus, the junction impedance effectively isolates the sub-systems, so one would not expect to see the

dynamics of the annulus sub-system in the main section of the liner. Also, since the dilution holes are so big, the theoretical basis for the junction impedance is probably no longer valid.

Another approach which seemed valid was to set up waves in the dilution holes. The problem with this approach is that the holes are very small in length and previous experience has shown that the pressure cannot effectively remain continuous in such a short length. From the inside of the liner, through the dilution holes, to the outer annulus there is a large area restriction and then a small area expansion. The area restriction of the dilution holes has a length equal to the thickness of the liner wall, thus there is basically a step change in pressure through the dilution holes making the pressure discontinuous. The final approach was to treat the plane at the dilution holes as a parallel path. Since the effective area of the four dilution holes is similar to the area of the annulus, the dilution holes and the annulus were modeled as one individual path. Figure 4.12b shows the BSC liner system response when the annulus is modeled as a parallel path. Again, the model captures the $\lambda/4$ and $3\lambda/4$ waves for the main section of the liner, but it also shows the annulus resonance near 350 Hz. This is a half-wave frequency based on a length of 17", but the geometry is not closed-closed as would be expected for a half-wave. The same wave can also be generated by an open-open geometry where pressure is nearly zero at each boundary. The boundary at the dilution holes looks "open" to the annulus because the area of the liner is over thirteen times the area of the dilution holes. Therefore, the proper way of modeling the dilution holes is to treat them as a boundary to match pressure and volume velocity between two wave elements.

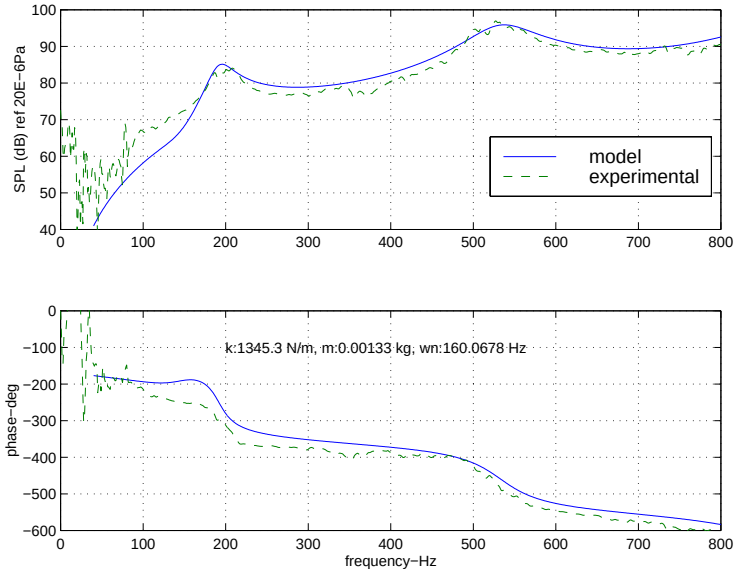

(a)

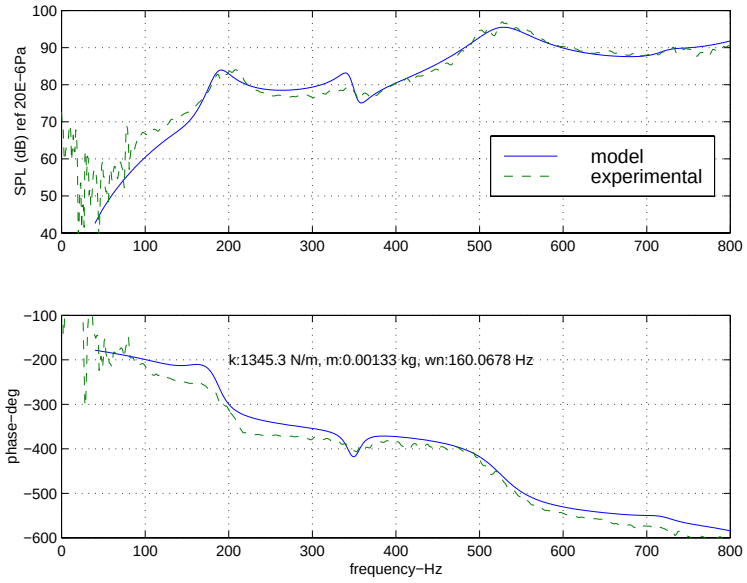

(b)

Figure 4.12 a,b-(a) FRF of backside cooled liner using a junction impedance to connect the annulus and the main section at the dilution holes. (b) FRF of backside cooled liner with annulus modeled as a parallel path at the dilution holes.

4.2-Full Rig Modeling with Inlet and Outlet Blocked

The tube and liner models provided the background information needed to model the entire rig which is shown in Figure 4.13. During the initial acoustic testing at Solar

Turbines it was found that the system response was modally dense, with peaks every 20 Hz. These low frequency waves were associated with the long lengths of inlet and outlet piping. To isolate the dynamics of the test rig's main section only, the inlet and outlet were blocked for the initial phase of testing. The inlet was blocked with a 1/16" thick aluminum blank inserted into a flange near the main section inlet. The outlet was blocked with a ½" thick piece of foam laminated between two pieces of ¾" plywood. These blockages contained most of the acoustic energy inside the main section of the rig where all the important dynamics (i.e. modes that should exhibit good coupling to the unsteady heat release) were located. This approach also made the system's frequency response much easier to model and analyze.

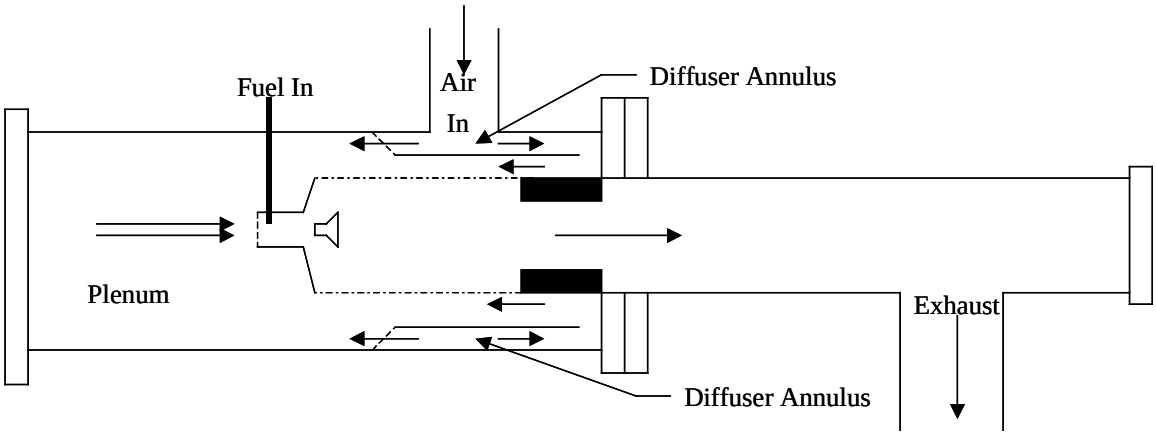

Figure 4.13-Schematic of single injector test rig.

4.2.1-Initial Full Rig Model

Figure 4.14 shows a diagram of how the blocked test rig was segmented into transmission line elements. The large number of elements in the combustor and annulus section are due to the need for a boundary at each plane where perforates exist. Increasing the number of elements drastically increases the computation time needed to invert the large coefficient matrix for all the frequencies in the bandwidth, but there is no option if good model fidelity is needed. The modeling is again done by matching pressure and volume velocity at the boundaries between each element. There are however, a few boundaries in the test rig which merit a more detailed discussion.

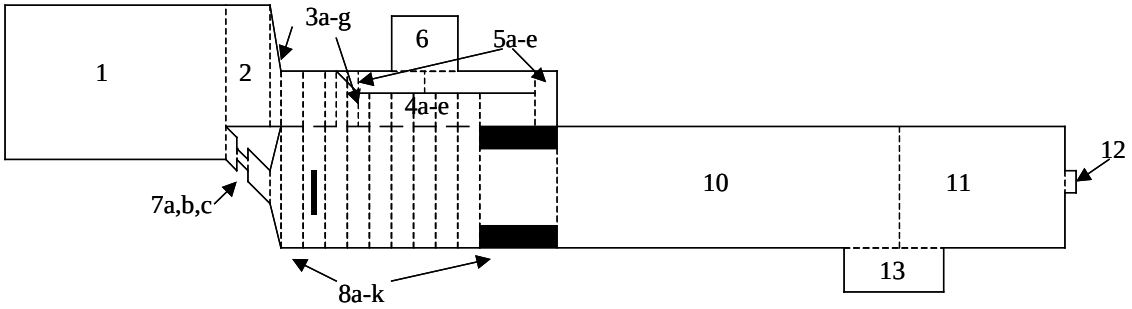

Figure 4.14-Element diagram of full rig with inlet and outlet blocked.

The critical areas identified in the initial modeling process were the injector (Sections 7a, b, and c), the perforated diffuser inlet (Sections 3f, 3g, 5a, and 5b), the end of the diffuser (Sections 4e, 5d, and 5e), and the inlet/outlet blockages (Sections 6 and 13). Figure 4.15 shows detailed drawings of each area and their boundary conditions. The injector was modeled assuming that the fuel spokes were choked since the fuel injection holes were very small, the swirler vanes were a simple area restriction, and the center body acoustics were out of the bandwidth being considered (See Section 4.1.3). These assumptions resulted in an injector model which consisted of a simple area restriction and expansion. A junction impedance was used to model the holes in the diffuser because the length of the holes were too short to generate waves, as discussed previously (Figure 4.15b). As Figure 4.15c shows, the end of the diffuser is an unusual boundary condition because it is difficult to determine what percentage of the wave energy reflects off the rigid boundary. The boundary was treated as a parallel path by matching the volume velocities on the left edge (Sections 4e, 5d, 5e), and setting the particle velocity to zero at the rigid boundary on the right edge of Section 5e.

The last complicated boundary of this model is the inlet and outlet blockages. It was known from the coherence of the experimental data that some energy was transmitted through these boundaries. Therefore, the most appropriate boundary condition would be a finite impedance, but a value for this impedance is very difficult to determine, so a rigid boundary condition was initially used.

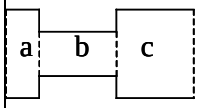

Boundary Conditions for Section 7a, b, and c:

- $P_{7a}(x=L_{7a})=P_{7b}(x=0)$, $P_{7b}(x=L_{7b})=P_{7c}(x=0)$
- $V_{7a}(x=L_{7a})S_{7a}=V_{7b}(x=0)S_{7b}$, $V_{7b}(x=L_{7b})S_{7b}=V_{7c}(x=0)S_{7c}$

where $S_{7b} = .8\ S_{7a}$ (Area reduction for swirler vanes)

(a)

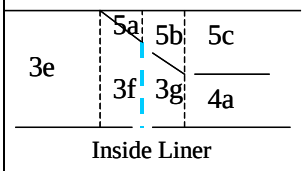

Boundary Conditions for Sections 3f-3g:

- $V_{3f}(x=L_{3f})S_{3f}=V_{3g}(x=0)S_{3g}+(P_{3f}-P_{8e})/Z_{junct\text{-}liner}+(P_{3f}-P_{5a})/Z_{junct\text{-}diff}$
- $P_{3f}(x=L_{3f})=P_{3g}(x=0)$

(b)

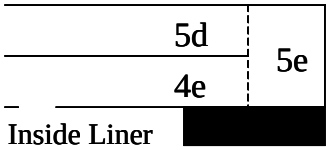

Boundary Conditions for Section 5e:

- $P_{4e}(x=L_{4e})=P_{5e}(x=0)$, $P_{5d}(x=L_{5d})=P_{5e}(x=0)$
- $V_{4e}(x=L_{4e})S_{4e}+V_{5d}(x=L_{5d})S_{5d}=V_{5e}(x=0)S_{5e}$
- $V_{5e}(x=L_{5e})=0$

(c)

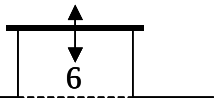

Modeling Approaches:

1-Rigid Boundary ($V_6(x=L_6)=0$)

2-Circular plate fixed around circumference

(d)

Figure 4.15 a, b, c, d- Critical boundary conditions and diagrams: (a) Injector element model. (b) End of diffuser element model. (c) Beginning of diffuser element model. (d) Inlet and outlet blockage modeling.

Assembling the 48 elements with the appropriate boundary conditions produces a FRF which shows the acoustic response of the system in the bandwidth of interest (0-450 Hz). This bandwidth is determined based on the fact that no instability frequencies are seen above 425 Hz when the test rig is at operating temperature and pressure. When the cold acoustic model is modified to account for the actual test rig operating conditions, the frequencies will be shifted higher by a factor of 1.5-2. A frequency of 425 Hz in the hot case will appear in the cold acoustic model around 240 Hz. Therefore, a cold acoustic model up to 450 Hz should have more than enough bandwidth to capture all of the acoustic dynamics needed to find the instability frequencies seen during the operation of the test rig. Figure 4.16 shows FRF's of the initial model after slight corrections in the

damping of the perforates in the liner. The model does well in capturing the dynamics of the test rig except for the region between 225-325 Hz. The only way to correct the model is to analyze the assumptions made for each particular geometry in order to determine if the assumption is valid or whether a more realistic assumption can be made.

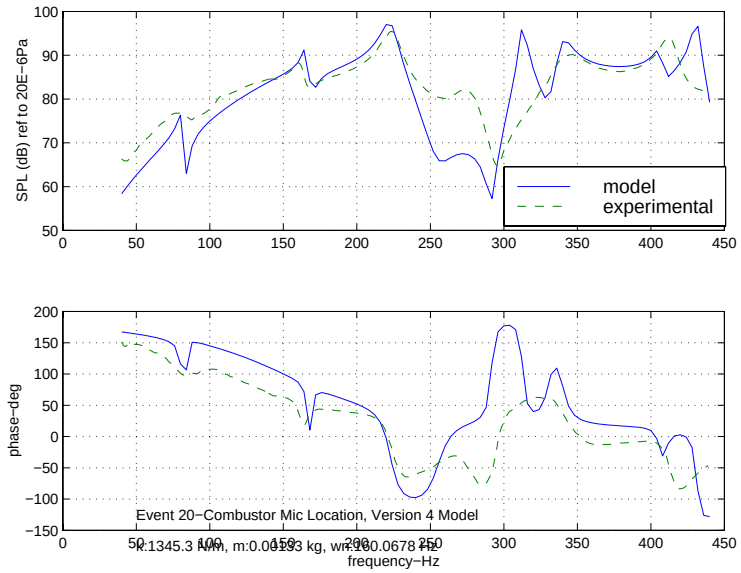

(a)

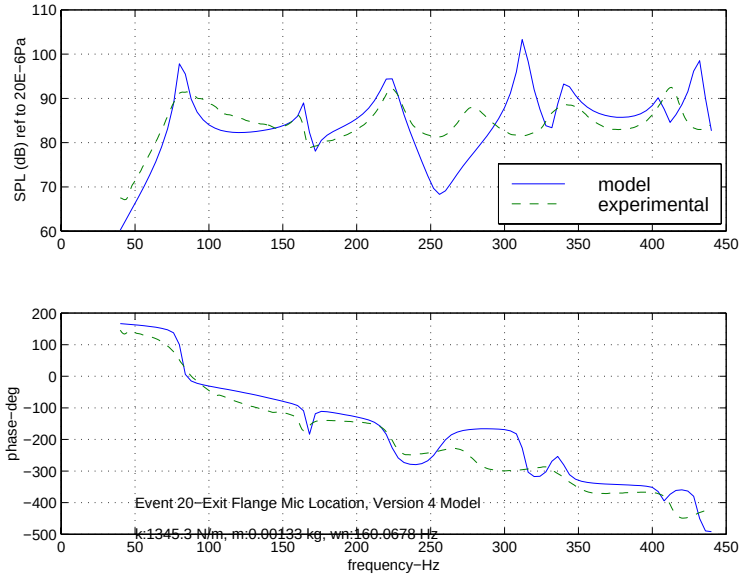

(b)

Figure 4.16 a,b-FRF of test rig with inlet and outlet blocked: (a) Combustor microphone location. (b) Exit flange microphone location.

4.2.2-Corrections to Full Rig Model w/ Blocked Inlet and Outlet

In order to correct the model, the critical boundary conditions identified previously were changed to see how the model's response changed. Table 4.1 lists the changes made to the model and the results of those changes. All of the changes focused on three major areas. Versions 2, 6, 7, and 10 all attempted to account for the lack of rigid boundaries at the inlet and outlet. Versions 3, 8, and 9 made changes to the diffuser annulus, and version 5 includes the more complicated injector model discussed in the injector modeling section.

Version	Changes Made to Baseline	Results
1	Baseline model.	Lightly damped peaks. Failure to follow data between 225-325 Hz.
2	Added % of ρc impedance at I/O based on coherence because of non-rigid boundary.	Damping increase, but very little change in resonant frequency location.
3	Changed BC of air diffuser to waves in small holes instead of Zjunct. Re(Zjunct) added to liner	Very little change in critical band (225-325 Hz). 160 Hz peak seems to disappear.
4	Re(Zjunct) added. P evaluated at mid-point of I/O.	Damping makes model match well with the data. P evaluated at mid-point slightly corrects peak location. NEW BASELINE
5	Complicated injector model used.	No change in low frequency. (<500 Hz)
6	Small volumes added in air plenum.	No change.
7	Small dia. Holes added at inlet to ver4.	Damping changed slightly. No significant change.
8	Added parallel path for trans. and reflect. at end of diffuser. (plus ver4 changes)	All peaks <225 Hz changed. 150 Hz peak greatly altered. Higher frequency remains unchanged.
9	Complete removal of diffuser (plus ver4 changes)	150 Hz peak moves to higher frequency (190 Hz). Other peaks change in amplitude.
10	Addition of clamped plate impedance and inlet boundary. (plus ver4 changes)	No change in low frequency. (<225 Hz) Slight correction in 225-325 Hz range.

Table 4.1-10 Versions of the full rig model with the inlet and outlet blocked.

The inlet and outlet boundary conditions were examined in great detail because it was known that some acoustic energy was being transmitted into the inlet and outlet piping sections based on coherence data taken between a microphone behind the blockage and the speaker input. In version 2, a frequency dependent percentage of the ρc impedance was added to the boundary conditions at the inlet and outlet. The percentage was determined based on the coherence. A coherence of 0 indicated that the boundary was rigid, while a coherence of 1 indicated that there was effectively no restriction at the boundary. Even though the coherence indicated a relatively high acoustic energy

transmission through the boundary in the 200-300 Hz band, adding a percentage of the ρc impedance failed to produce the desired change in the model. Another attempt at modeling the non-rigid boundaries was to add a small hole in the boundaries. The goal was to allow a path for energy dissipation without allowing the dynamics of the inlet and outlet piping into the main section. This added damping to the system, but did not affect the location of the resonant frequencies. The last attempt to model the inlet and outlet boundaries was to actually model the dynamics of the plate. Equation 4.5 is a theoretical mechanical impedance used to model a clamped circular plate and also an approximate value for the first natural frequency of the plate from Timoshenko [31]. It was thought that the acoustic waves would excite the plate near the natural frequency of the plate, thus transferring energy through the plate to the other side where it would act like a piston source to excite the waves in the inlet piping. Away from the natural frequency, the acoustic waves would not be able to excite the plate, therefore it would act as a rigid boundary. This would explain the bands of good and bad coherence seen in the experimental data. The plate impedance shifted the frequencies in the range between 200-350 Hz, but these corrections adversely affected other parts of the response. After numerous attempts at modeling the non-rigid inlet and outlet boundaries it was concluded that there was insufficient test results to model the actual system, so the rigid boundary condition was used for the rest of the study.

$$Z_{mech} = \frac{M}{4j\omega}(\omega^2 - \omega_{11}^2)$$

$$\omega_{11} = \frac{\alpha}{a^2}\sqrt{\frac{D}{\rho h}}, \alpha = 10.21, D = \frac{Eh^3}{12(1-\nu^2)} \quad (4.5)$$

Another critical area was the annulus around the combustion liner. The dynamics of this section in and of itself is not that important, but since the pressure field in the annulus outside the liner partially determines the junction impedance for the perforates of the liner, it is important to have the correct pressure field in the annulus. In version 3, the junction impedance for the diffuser holes (sections 5a, b) was replaced by wave elements to allow waves to be transmitted from the inlet plenum (sections 2,3) to the diffuser

annulus (section 5). The problem with this approach is that, in order to establish waves in these sections, the lengths of each section must be made unrealistically long in order to allow the pressure to transition across the element. If the length of the diffuser hole elements is increased, then the version 3 model looks very similar to the junction impedance model except that the peak near 150 Hz no longer appears. Because one of the system acoustic modes was lost when using waves in the diffuser holes, it was concluded that the junction impedance was indeed the proper boundary condition. The other attempted modification was implemented at the end of the diffuser where sections 4 and 5 join together. A parallel path was created to allow for both reflection of the wave at the rigid boundary, and transmission of the wave around the end of the boundary. The parallel path approach resulted in changes very similar to the response seen for version 3. Again, this modification did not result in a better model, therefore the original boundary conditions were assumed valid.

The last critical geometry investigated was the injector. From the injector modeling section it was known that the injector itself had only high frequency dynamics. However, it was thought that the complex injector model may affect the lower frequency response of the system by changing the impedance at the injector boundary. The complex injector model produced no changes to the system model, showing that the injector affects only the higher frequency system dynamics.

After having very little success correcting the model in the bandwidth of interest, a general overview was made of the entire test rig model to identify if any large scale problems were being overlooked in the detailed analysis which was being conducted. The result of this overview was a new approach of trying to identify which acoustic modes were related to specific geometric features of the test rig. If these geometries could be identified, then the corrective measures could focus on these specific areas in the test rig. Knowing which geometries were linked to specific modes would provide the ability to control the mode's response. In order to accomplish this task, a simplified rig model was constructed which maintained all the dimensions of the test rig, but eliminated many of the finer details such as the diffuser and small area changes.

4.2.3-Analysis of Acoustic Mode Origins with Inlet and Outlet Blocked

Creating a simplified rig model allows the boundary conditions to be as simple as possible. Simple boundary conditions result in acoustic resonances near theoretical ½ and ¼ wave frequencies. Once an acoustic mode can be associated with a specific geometry, more complicated boundaries can be added one-by-one to see how they affect the theoretical ½ and ¼ wave frequencies. Figure 4.17 shows the transmission line elements used to model the simplified rig. The theoretical ½ wave frequencies associated with the rig geometry are shown in Table 4.2.

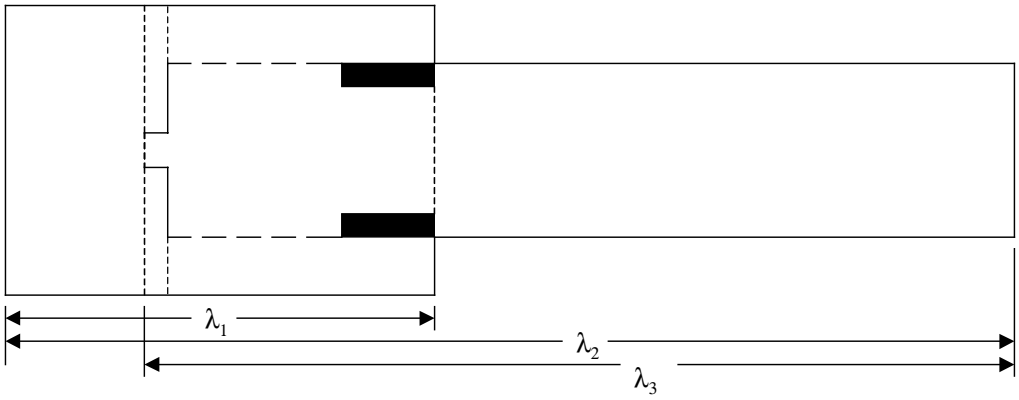

Figure 4.17-Schematic of the simplified test rig.

Theoretical Values:
$\lambda_1/2$=199 Hz, λ_1=397 Hz, $3\lambda_1/2$=597 Hz
$\lambda_2/2$=113 Hz, λ_2=226 Hz, $3\lambda_2/2$=340 Hz
$\lambda_3/2$=151 Hz, λ_3=312 Hz, $3\lambda_3/2$=468 Hz

Table 4.2 - ½ Wave frequencies associated with simplified test rig.

Figure 4.18 shows an FRF of the simplified test rig with labels for each of the identified acoustic modes. Many of the peaks are very close to the theoretical ½ wave frequencies, and the amplitude of certain peaks are highly dependent on the measurement location. With these two observations in mind, each peak was initially identified and then certain aspects of the model were changed in order to prove which rig geometries were associated with each acoustic mode.

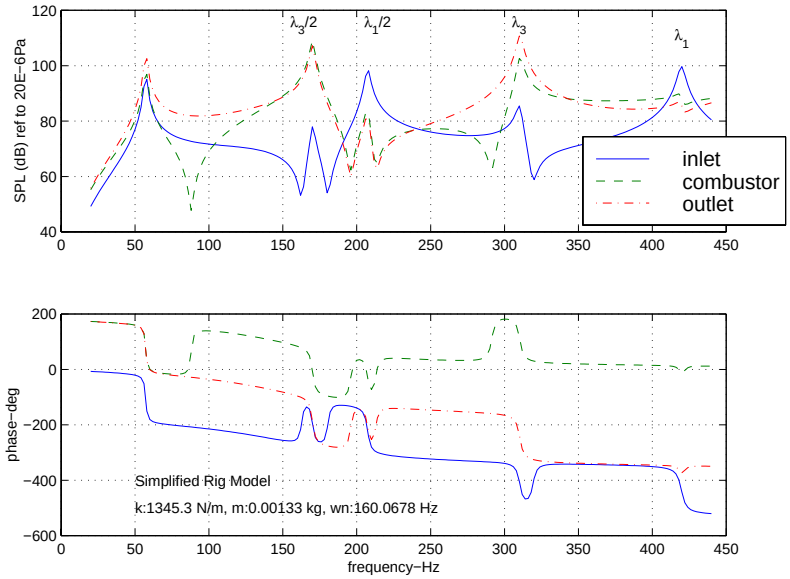

Figure 4.18-FRF of simplified rig with the inlet and outlet blocked and no perforates.

The first peaks identified were those near 210 and 420 Hz. These two peaks agreed well with half and full waves in the inlet section of the test rig. Figure 4.18 provides further evidence to this hypothesis since the amplitude for these peaks is much higher at the inlet microphone location than the combustor and outlet microphones. Figure 4.19 shows how the system response changes when the annulus of the inlet section is removed. The 210 and 420 Hz peaks no longer appear in the response, thus it can be concluded that these peaks are associated with the inlet section of the simplified rig.

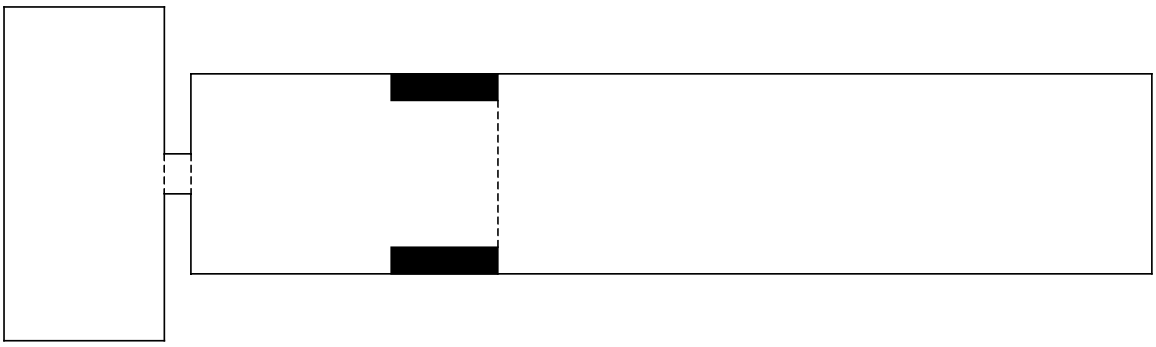

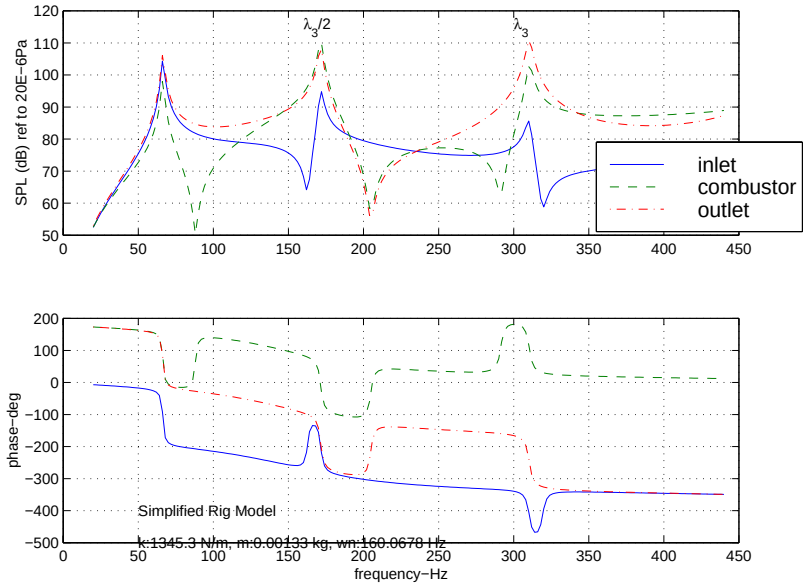

Figure 4.19-Schematic and FRF of simplified rig with inlet and outlet blocked, no inlet annulus, and no perforates.

The next two peaks investigated were the ones at 170 and 310 Hz. These two frequencies are very close to the theoretical half and full-wave frequencies of the combustor-outlet section of the simplified rig. Figure 4.19 provides more information to substantiate this claim because the 170 and 310 Hz peaks are not affected by changes to the inlet. To show this more directly the entire inlet section was removed. Figure 4.20 shows the system response with only the injector, combustor, and outlet sections. Again, the previously identified inlet peaks do not appear, as expected, but also the 170 and 310 Hz peaks remain unchanged. Therefore, the only geometry that can create these waves is the combustor-outlet section. Figure 4.20 also shows that the injector geometry virtually isolates the dynamics of the inlet section from the dynamics of the combustor-outlet section. This is not surprising since the area ratio between the inlet plenum and the injector is greater than 25, thus the inlet plenum is so 'big' that it looks like an open boundary to the injector. Also, the area ratio between the combustor and the injector is 10, so the boundary at the injector face looks mostly like a closed boundary to the combustor-outlet section. This is a very important conclusion since it shows that the dynamics of the combustor is governed almost exclusively by the geometry down stream of the injector.

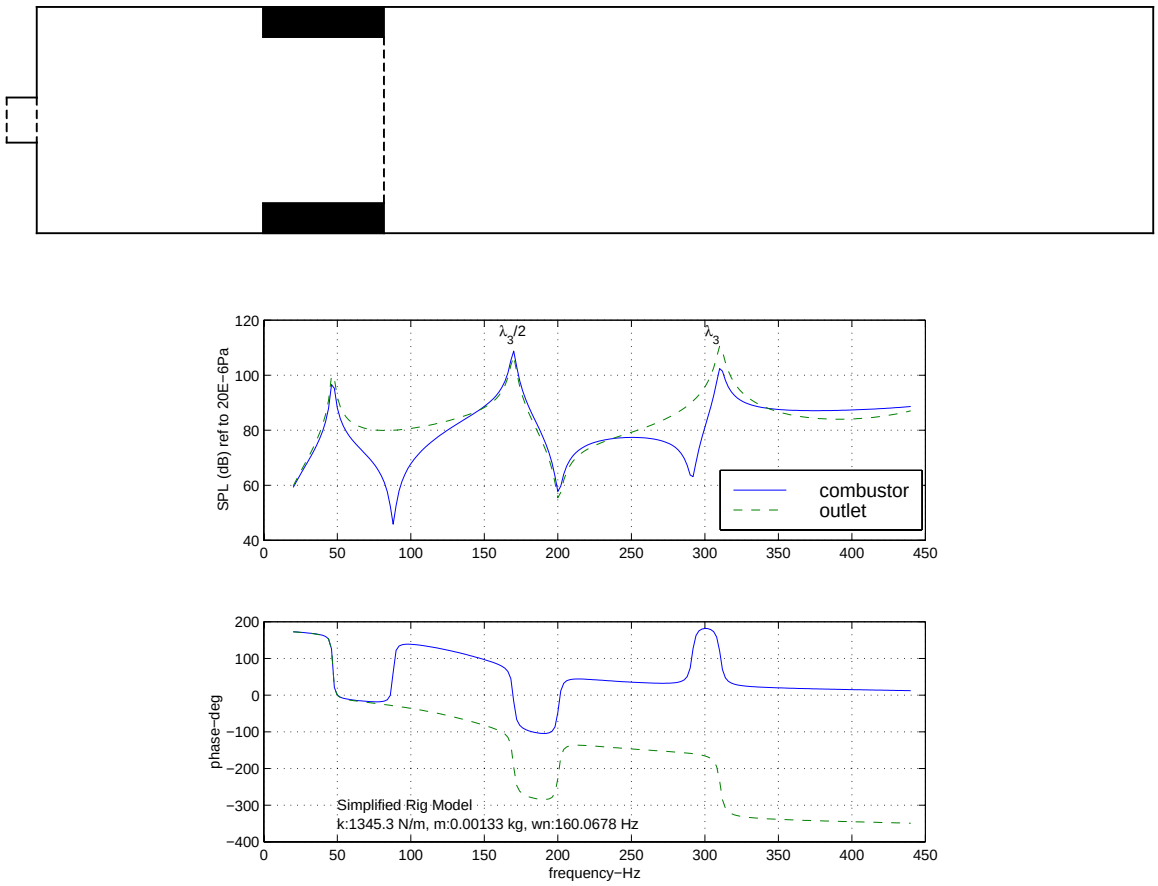

Figure 4.20-Schematic and FRF of simplified rig with inlet and outlet blocked, no inlet plenum, and no perforates.

Even with the previous conclusions, the inlet section of the test rig must still be modeled because the combustion liner communicates with the inlet annulus through the cooling holes in the liner. To investigate how the perforates influenced the response, additional rows of holes were added to the liner. Figure 4.21a,b show the addition of two and four rows of holes, respectively, to the original simplified model. Comparing these plots with Figure 4.18 shows that the 55, 170, and 310 Hz waves move to higher frequencies, while the inlet section modes (210 and 420 Hz) change very little. Thus, the perforates in the liner move the theoretical ½ wave frequencies higher.

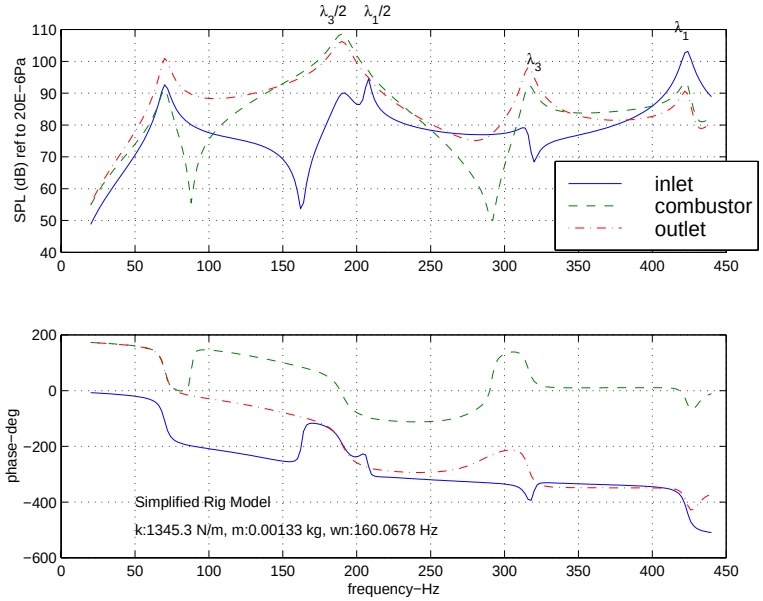

(a)

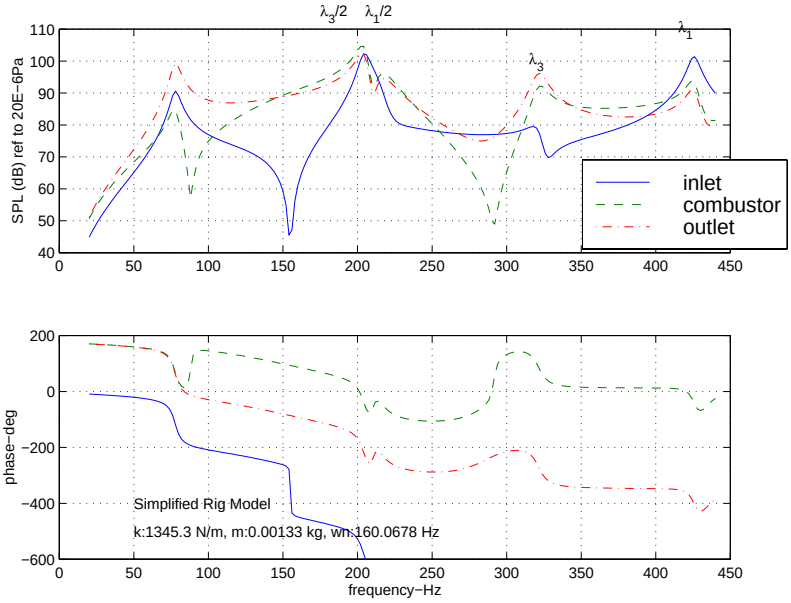

(b)

Figure 4.21 a,b- (a) FRF of simplified rig with inlet and outlet blocked and 2 rows of perforates. (b) Simplified rig with inlet and outlet blocked and 4 rows of perforates.

The previous discussion has focused little on the lowest frequency peak seen in the spectrum near 55 Hz. This mode could be associated with the whole system even though it is not close to the theoretical ½ wave rig frequency of 113 Hz. This hypothesis is supported by noticing that the inlet and outlet microphone locations are out of phase.

The disparity in frequency could be due to the drastic area restriction and expansion at the injector boundary. The basis for this possible conclusion comes from the theoretical study discussed in chapter 3, which showed that area changes can drastically affect the frequency of an expected ½ or ¼ wave.

Another explanation could be that the injector, combustor, and outlet sections act as a Helmholtz resonator. The injector would serve as the resonator neck, and the combustor-outlet section would be the volume. Using these dimensions the theoretical Helmholtz frequency is 46 Hz. The combustor and outlet microphones being in phase also supports the idea of a bulk Helmholtz mode. The simplified rig FRF's show that this frequency moves with changes to the inlet section and the addition of perforates. The FRF with the inlet completely removed (Figure 4.20) has a frequency closest to the theoretical Helmholtz frequency. This geometry also most closely matches that of an ideal Helmholtz resonator. The other models provide a different impedance at the injector opening, thus shifting the expected Helmholtz frequency.

In an attempt to prove the origin of this low frequency mode, ten additional inches was added to the inlet plenum. The goal was to lengthen the entire rig while not changing the geometry of the resonator. If the peak shifted, then it could be concluded that it was a full rig mode, but if there was no change to the frequency then it could be identified as a bulk mode. Changing the length of the rig changed the frequency by only 4 Hz, thus strongly indicating that this frequency is most likely due to a bulk Helmholtz mode based on the combustor-outlet section.

Based on the identified peaks in the simplified rig the modes in the test rig with the inlet and outlet blocked can be identified. Comparing Figure 4.21b and Figure 4.16 shows that the perforates have moved the low frequency bulk mode (55->82 Hz) and the ½ wave in the combustor-outlet section (155->220 Hz) to higher frequencies. The ½ wave frequency associated with the inlet section (210->160 Hz) decreases because the diffuser adds additional length to the ½ wave. Analysis of the higher frequency modes becomes much more difficult since the model fails to correctly predict the system's response. Based on the knowledge gained from the simplified rig, numerous changes were made to almost all the geometries of the test rig, but none of these changes resulted in a better model than the comparisons shown in Figure 4.16.

Even though the injector isolates the inlet section from the combustor-outlet section, the perforates allow the pressure field in the inlet section to affect the impedance seen by the waves in the combustor. The modeling of the combustor has been validated in the component testing, and the outlet section is simply a pipe, so it would appear that the model is failing to capture the proper dynamics in the inlet annulus where the diffuser section is located. To concluded this section, it is believed that the model is not predicting the correct response in certain bands because it fails to predict the proper pressure distribution in the annulus, resulting in the wrong junction impedance on the liner.

4.3-Helmholtz Resonators

In this chapter, much has been mentioned about a louver liner with a refractory plug. The plug is an adaptation to the louver liner in an attempt to create a Helmholtz resonator. A Helmholtz resonator is an acoustic lumped element which consists of a closed cavity with a small neck on one end. In the neck, the air moves as a slug of fluid providing the mass element for the resonator. If the pressure oscillation at the neck opening is thought of as a piston being displaced, then the closed volume acts as the piston's stiffness. Resonance of a mechanical system is known to occur when the reactive part of the mechanical impedance equals zero, which in this case results in Equation 4.6. Resonance is based solely on geometric considerations including the cavity volume (V), the mass radiated corrected length of the neck (L'), and the area of the neck (S).

$$\omega_0 = c\left(\frac{S}{L'V}\right)^{\frac{1}{2}} \quad (4.6)$$

The goal of installing a ceramic plug was to design the combustion liner as a Helmholtz resonator so that there would be a preferred frequency of oscillation inside the liner. The target frequency was a frequency which generated high amplitude pressure oscillations in a full-scale engine. The hypothesis was that, if an injector design failed to

excite a frequency which was preferred inside the liner, then it would not excite that frequency in the full engine. The goal of this work is to use the model to see if the louver liner geometry does represent a Helmholtz resonator. Because the liner is part of the test rig, its acoustic interaction with the rest of the rig must be taken into account. Therefore, the model must account for how other geometries of the test rig affect the liner's ability to generate a Helmholtz frequency.

Knowing that the injector isolates the inlet plenum from the combustor-outlet section, a simplified Helmholtz model can be constructed simply with the combustor and outlet sections. To idealize the model, the injector face will be modeled as a rigid wall and no perforates will be included. Figure 4.22 shows the simplified geometry which represents the 17.8" long combustion liner and the outlet section. The diameter of the plug (d), and the length of the outlet section (l) will be varied in order to show how well the plug creates a preferred frequency in the combustion liner.

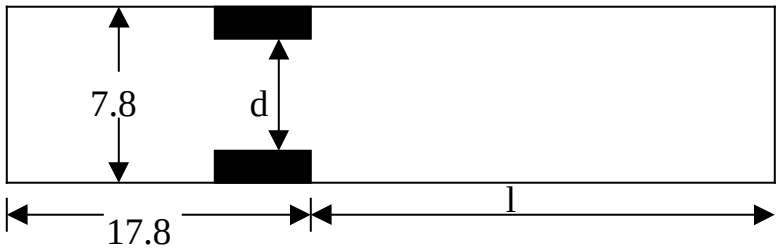

Figure 4.22-Schematic of simplified Helmholtz geometry in test rig.

The baseline model has no plug (d=7.8") and an outlet section length of 25.5". Figure 4.23 shows the FRF of this system. Without a plug, this is a simple closed-closed tube and, as would be expected, the two resonant frequencies of 158 Hz and 316 Hz correspond to half and full-wave frequencies based on the entire length. The next model duplicates the actual configuration of the test rig by making the plug diameter 5.72", while maintaining an outlet section length at 25.5". As Figure 4.24a shows, the frequencies shift slightly lower. This slight change is consistent with an area restriction, but the lowest resonance is near the Helmholtz frequency of 128 Hz based on the combustor geometry. By varying the length of the outlet section it will be easy to make a conclusion about the origin of the first acoustic resonance. Reducing the length of the outlet section would move the expected half-wave frequency higher. Since the

Helmholtz frequency is completely dependent on the combustor geometry, changing the length of the outlet section should have little affect on the Helmholtz frequency. Figure 4.24b shows that when the length of the outlet section is reduced by 10" both resonant frequencies move higher. The conclusions from this study show that the acoustic resonances are based on half and full-waves in the entire section, and not a bulk Helmholtz resonance in the combustor.

To further investigate the Helmholtz bulk element the diameter of the plug was reduced to 2", while the length of the outlet section was 25.5". The resulting FRF in Figure 4.24c shows two interesting characteristics. First, there is a lower than expected resonant frequency at 77 Hz, and secondly, a higher than expected resonant frequency at 272 Hz based on the length of the entire rig. It can be hypothesized that the plug diameter has been reduced enough to de-couple the combustor from the outlet section, therefore allowing a Helmholtz frequency to form. As a result of the de-coupling, half-waves form only in the outlet section. With these two hypothesizes in mind, one would expect that reducing the length of the outlet section would not affect the lowest frequency resonance since it has been assumed to be the Helmholtz frequency. Also, the highest frequency resonance would move higher because of the reduced length of the outlet section. Figure 4.24d shows the result of reducing the length of the outlet section by 10" while maintaining the 2" plug diameter. The low frequency peak is affected very little by the reduction in length of the outlet section, indicating that the combustor is a Helmholtz resonator. The highest frequency resonance moves to a much higher value, showing that this acoustic resonance depends on the outlet section. Another observation which validates these conclusions is that the high frequency peak is only measured by the outlet section microphone.

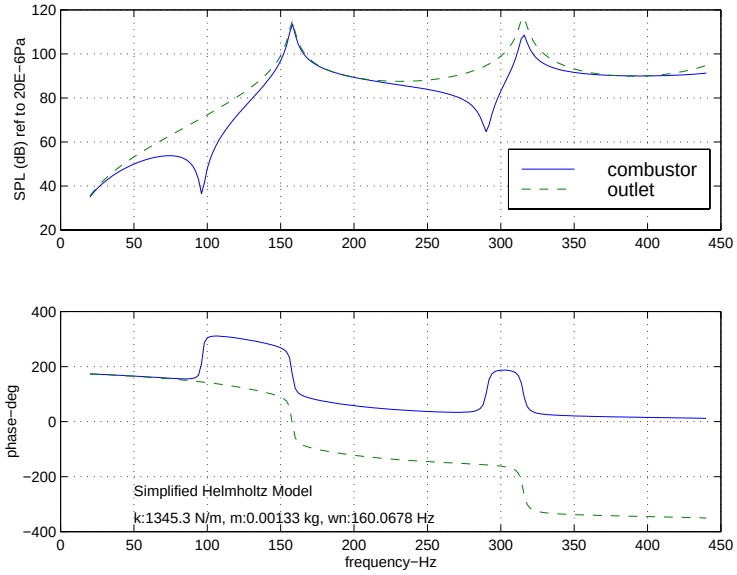

Figure 4.23-Baseline Helmholtz model with d=7.8” and l=25.5”.

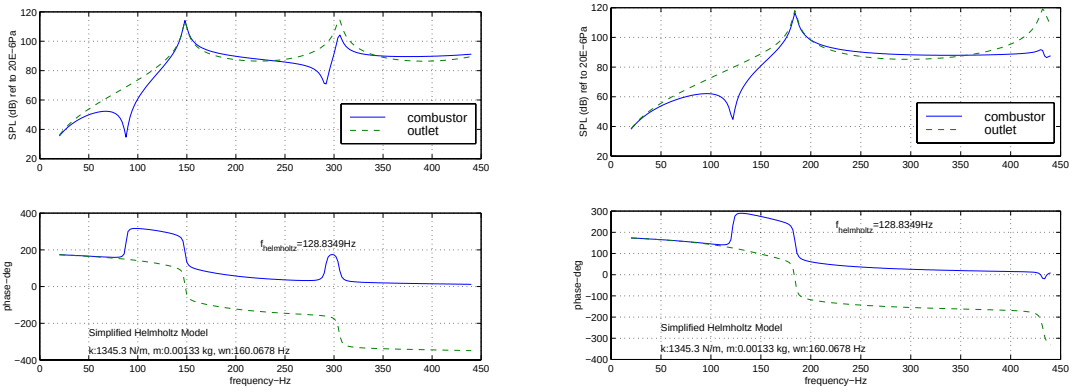

(a) (b)

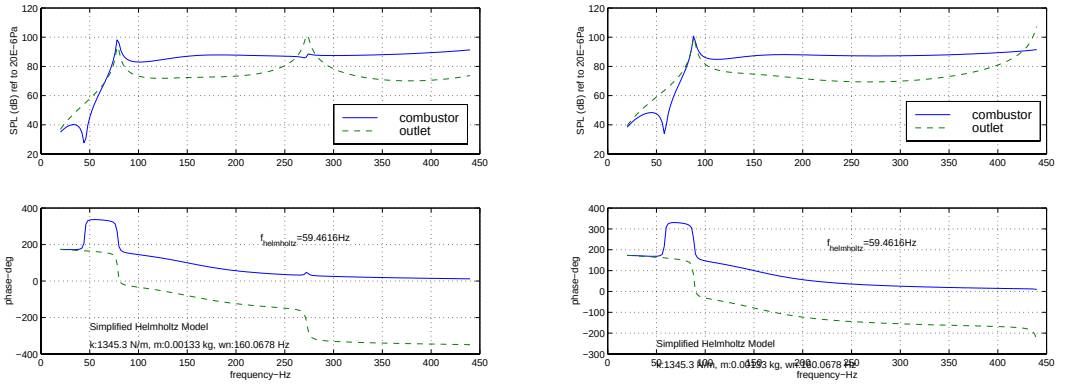

(c) (d)

Figure 4.24 a, b, c, d-FRF’s of simplified Helmholtz model: (a) d=5.72”, l=25.5”. (b) d=5.72”, l=15.5”. (c) d=2”, l=25.5. (d) d=2”, l=15.5”.

It can be concluded from the Helmholtz model study that the current configuration of the louver liner with a plug does not act as a Helmholtz resonator. Helmholtz resonators are designed with the assumption that they are radiating into open air. If a resonator is used in a closed system the area ratio between the resonator neck (plug) and the area it opens into must be large. With a plug diameter of 5.72" the area ratio between the plug and the outlet section is too small to isolate the resonator, so instead it is coupled with the rest of the system and the plug acts only as a simple area restriction. When the plug diameter is reduced to 2", the area ratio is large enough to mostly isolate the combustor, allowing the formation of a bulk Helmholtz resonator. The injector opening could also affect the combustor's ability to form a bulk Helmholtz element. Remembering that the closed volume of the liner acts as a stiffness, it is easy to see that adding a hole for the injector would destroy the closed volume. The results of this study indicate that designing a Helmholtz resonator using the combustion liner would be very difficult since the liner must be designed for combustion purposes and not purely for its acoustic properties.

4.4-Full Rig Modeling

The rig model with the inlet and outlet blocked captured the main section acoustics, but to completely capture all of the acoustic dynamics the inlet and outlet piping must be added to the model. Adding the inlet and outlet piping to the model is a very simple task since only a few sections of constant area pipe must be added. Figure 4.25 shows the entire system response including the inlet and outlet piping. The additional length of the system increases the acoustic mode density in the bandwidth, especially at the inlet microphone location. The model again fails to capture the dynamics from 225-325 Hz. This indicates that the problems in the main section rig model also exist in the entire rig model. Since the additional transmission line elements are so simple, there are very few new changes which can be made to this model. Identifying the origins of the acoustic modes though, will provide some information about the dominant acoustic geometries.

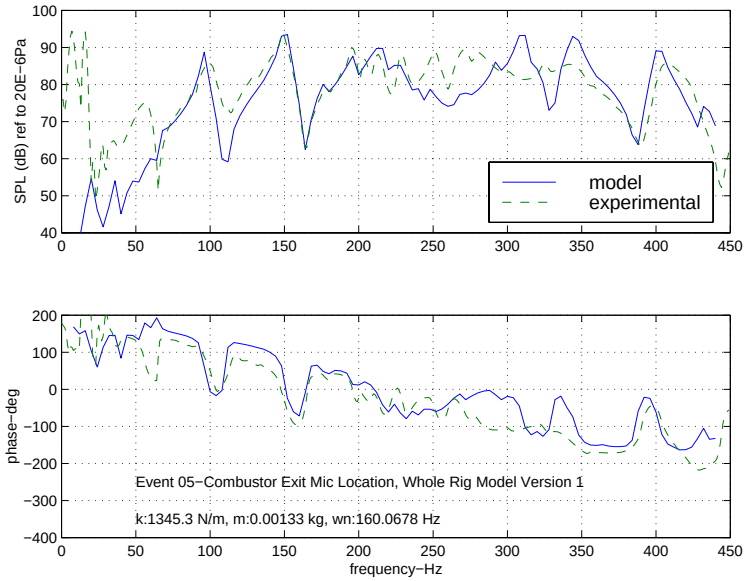

(a)

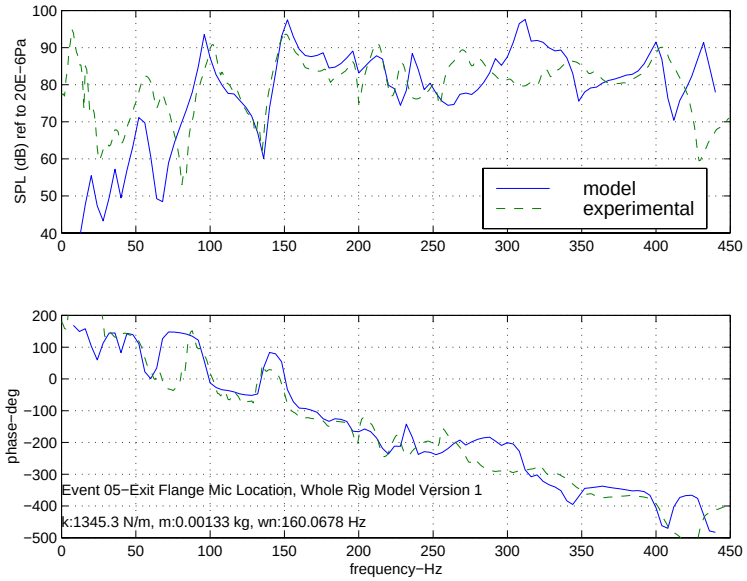

(b)

Figure 4.25 a, b- FRF's of entire rig with inlet and outlet piping: (a) Combustor exit microphone location. (b) Exit flange microphone location.

4.4.1 -Analysis of Acoustic Mode Origins for Full Rig

In order to identify the acoustic modes in the band from 0-450 Hz, inlet and outlet lengths were added to the simplified model used for the main section of the rig. Adding incremental lengths to the inlet, then to the outlet, and finally to both showed how the

acoustic modes changed in relation to their locations in the main section simplified model. Figure 4.26 shows a simplified rig schematic and the system response with and without the inlet piping. Both cases have four rows of perforates in the liner and no outlet piping. These FRF's show that, even with additional inlet piping, the main section acoustic modes still dominate the response. The inlet piping acoustics superimposes closely spaced acoustic modes onto the main section acoustics. As with the main section simplified model, the injector element isolates the inlet section from the combustor-exit section. This can be seen in the response by noticing that the closely spaced inlet piping resonances are distinctly apparent only at the inlet microphone location. Both the combustor and exit microphone locations capture only the main section dynamics. Because the acoustic response of interest is in the combustor, the section affecting the combustor's response the most is not the inlet section, but rather the outlet section.

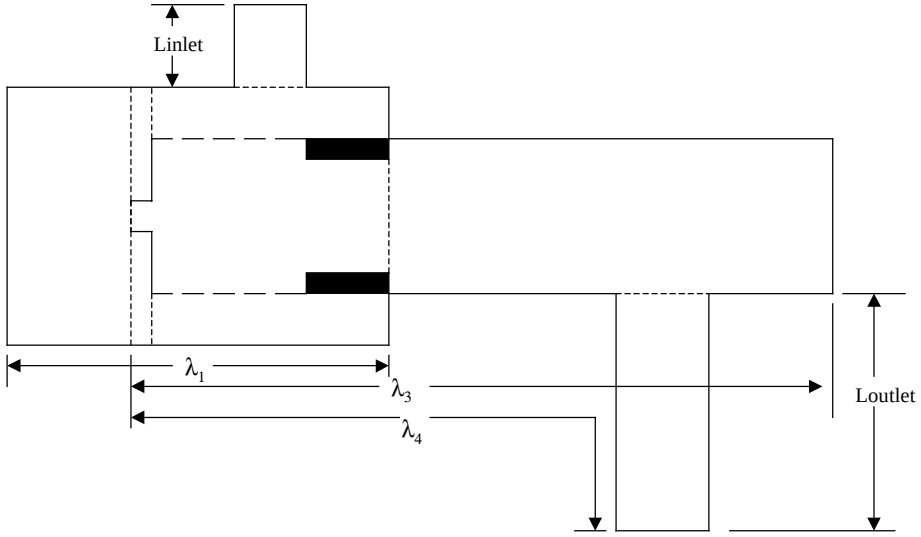

(a)

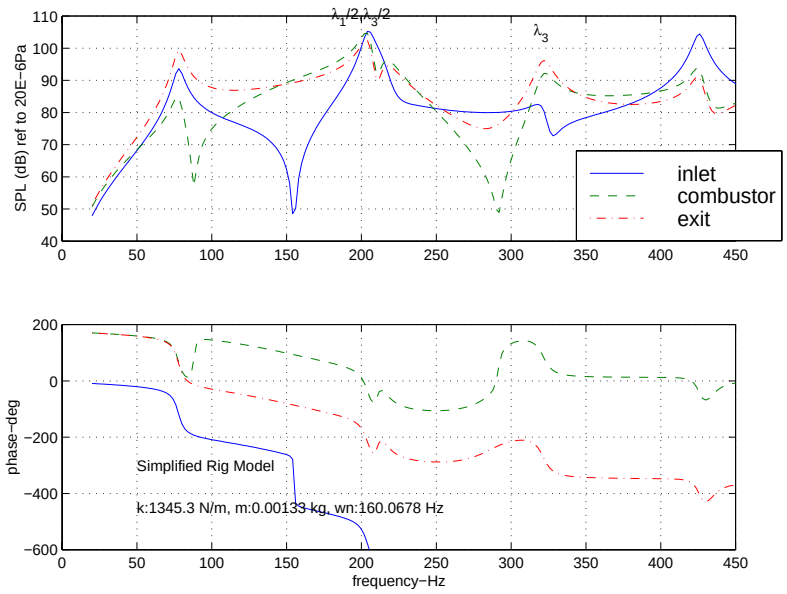

(b)

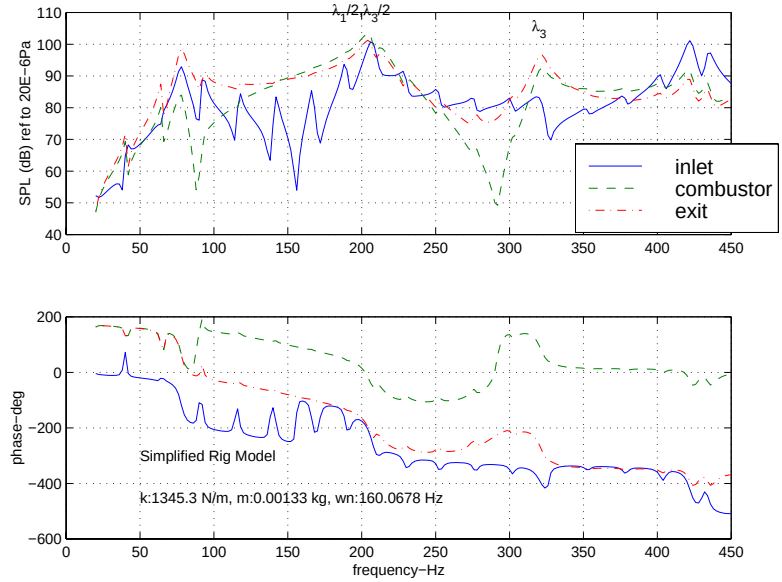

(c)

Figure 4.26 a,b- (a) Schematic of simplified rig. (b) FRF of simplified rig with 4 rows of perforates, Linlet=0", and Loutlet=0". (c) FRF of simplified rig with 4 rows of perforates, Linlet =260", and Loutlet=0".

To investigate the affect of the outlet piping on the main section, the inlet section was initially blocked. Figure 4.27a shows how the outlet piping adds to the main section dynamics, as compared to Figure 4.26 which has no inlet or outlet piping. Unlike the

inlet piping, the outlet does change the main section dynamics substantially. The main section modes still occur, but there are additional modes formed from the injector to the back-pressure valve at the end of the exhaust piping. The acoustic mode frequencies do not occur exactly where one would expect to see half-wave frequencies because the main section and the exit piping form a parallel path which divides the acoustic pressure, much the same way as current is divided between parallel paths in an electrical circuit. In order to identify the origin of each acoustic mode in Figure 4.27, the main section length was changed to see which peaks were affected. From repeated tests, the modes which moved were known to be half-waves forming from the injector to the exit flange. The other peaks were identified by watching them shift in frequency as the outlet piping length was changed. All of the major peaks were identified in the band of interest except the lowest frequency peak which is thought to be a bulk mode, but no conclusive evidence could be found to support this claim. Figure 4.27b again shows that the injector isolates the combustor-outlet section from the acoustic waves that form in the long inlet pipe. The inlet microphone shows the densely spaced acoustic modes which are a result of the long inlet section. The acoustics downstream of the injector are dominated by the combustor-outlet geometry.

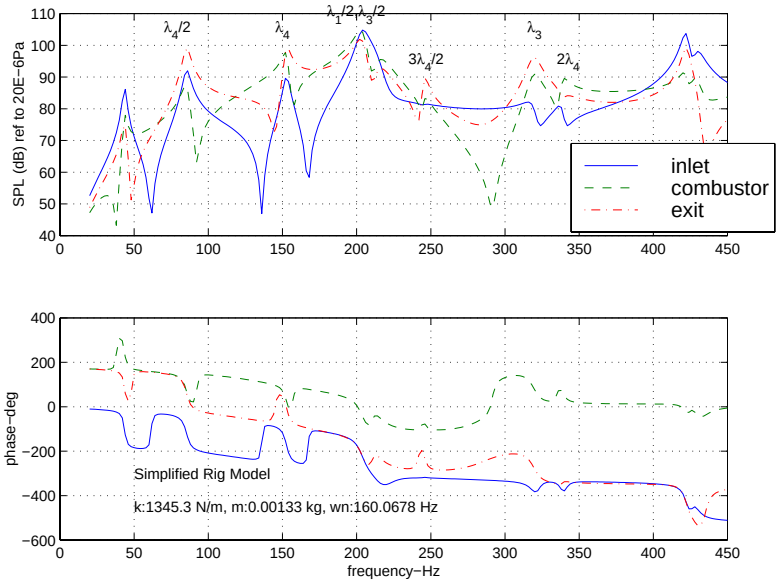

(a)

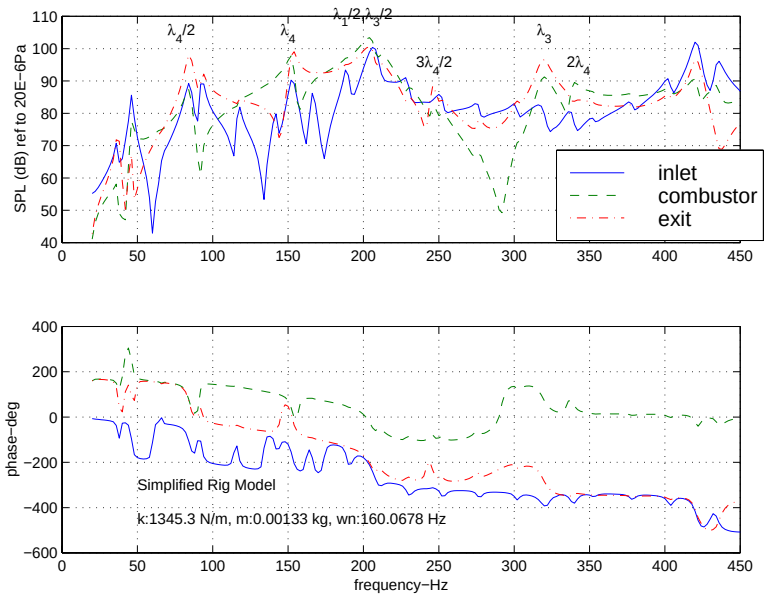

(b)

Figure 4.27 a,b- Simplified rig with 4 rows of perforates: (a) Linlet=0" and Loutlet=70". (b) Linlet=260" and Loutlet=70".

Using the knowledge gained with the simplified rig the distinct peaks in the full rig model were identified. This is not a simple task since there are so many peaks in the bandwidth being considered and the model does not match exactly with the experimental data. The only substantial difference between the simplified rig and the full rig is the number of perforates in the liner which increases the frequencies seen in the combustor-outlet section. Comparing Figures 4.25 and 4.27 one can see that $\lambda_4/2$ moves from 85 Hz to 100 Hz, λ_4 remains nearly fixed near 150 Hz, and $\lambda_3/2$ moves up slightly from 200 Hz to 220 Hz. Based on the system's response to length changes, and the assumption of which modes should be dominate, these identifications are the best which can be made at this time.

The errors plaguing the main section rig model also seem to plague the full rig model. After attempting to correct the errors in both models it was decided that, in order to complete the project in a reasonable time frame, these models would have to be good enough. Even though these models do not match the data between 225 and 325 Hz, they do match the actual dynamics up to 225 Hz. Depending on the temperature scaling, the 225 Hz frequency could be scaled to nearly 400 Hz. Since the highest instability

frequency seen during operation is 425 Hz, the current model should be able to capture all of the actual acoustic dynamics up to nearly 425 Hz.

4.5-Full Rig Model with Backside Cooled (BSC) Liner

Another standard testing configuration is the BSC liner in the test rig. The knowledge gained from the BSC liner modeling in Section 4.1.5 made the BSC liner's insertion into the test rig model very simple. Compared with the louver liner, there are fewer boundary conditions due to the lack of a perforated liner wall. The only difference from the liner component modeling is that the radiation impedances at the liner exit and the cooling jacket annulus are replaced with pressure and volume velocity boundary conditions which match those of the surrounding elements. With these adjustments Figure 4.28 shows the resulting frequency response of the BSC liner test rig with the inlet and outlet blocked.

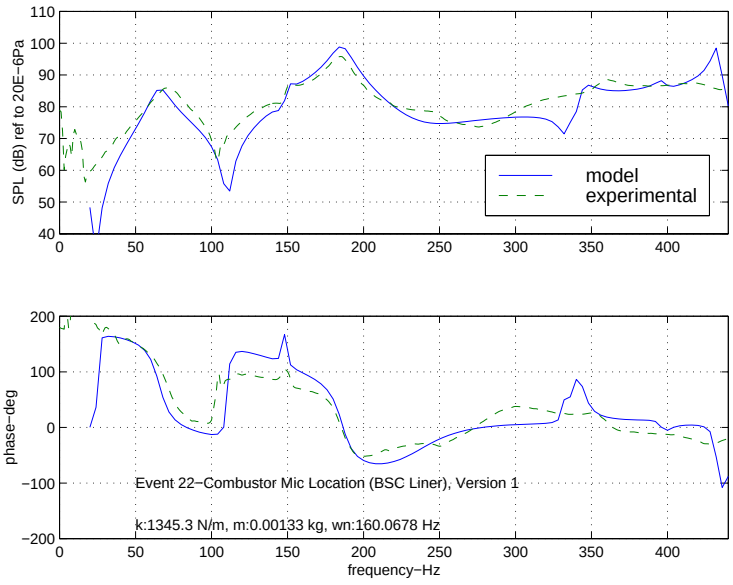

(a)

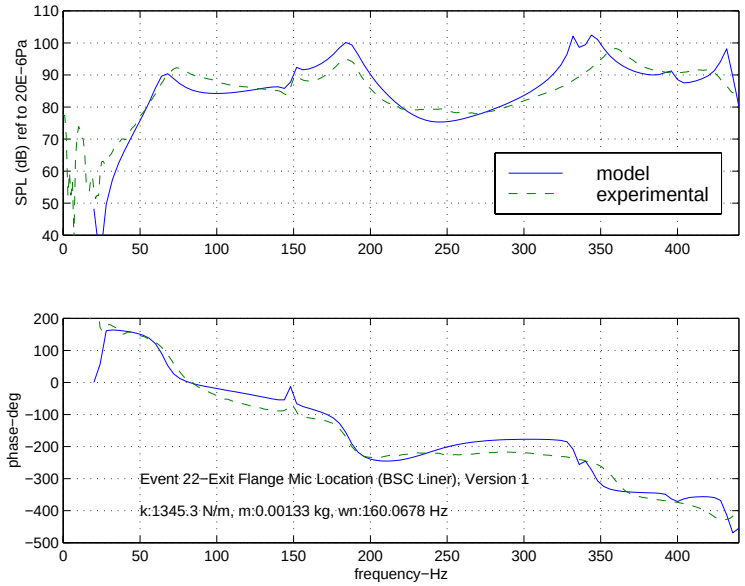

(b)

Figure 4.28a,b-FRF of test rig with inlet and outlet blocked and BSC liner: (a) Combustor microphone location. (b) Exit flange microphone location.

The BSC liner test rig model matches very well with the experimental data. The model should predict the response better than the louver liner model since the BSC liner model has fewer boundary conditions, thus making it simpler.

Based on the louver liner models, it is easy to identify the major peaks in the spectrum. As with previous models, the resulting spectrum indicates that the injector acts as a nearly rigid boundary, generating dominant waves either in the inlet section or the combustor/outlet section. Referring again to Figure 4.28, the 150 Hz peak, which is most pronounced at the inlet flange microphone, is a half-wave from the inlet plenum to the diffuser annulus section. The 180 Hz peak is a half-wave formed from the injector to the exit flange, with its corresponding full-wave frequency occurring near 360 Hz. Even though there is no experimental data to verify the assumption, one would expect that when the inlet and outlet blockages were removed the important lengths in the combustor-outlet section would be from the injector to the exit flange and the backpressure valve, as was seen with the louver liner model. Because the BSC liner test rig model matches the data to 300 Hz, it should provide a very accurate acoustic model up to 425 Hz when the acoustics are scaled to the operating conditions of the test rig.

4.6-Scaling Acoustics to Actual Operating Conditions

The acoustics modeled previously have been based on standard temperature and pressure (STP), but the actual combustion process takes place at an elevated temperature and pressure. As shown in Equations 4.7a and b, the temperature and pressure affect both the fluid density and also its speed of sound. Therefore all of the parameters dependent on ρ and c, i.e. the characteristic acoustic impedance (Z) and the wave number (k), will be affected. Changing the mean pressure is very straightforward since it is uniform inside the rig, but the temperature varies for specific sections of the rig since the air is heated by the flame, and is then cooled through the use of cooling air and water sprays.

$$\rho = \frac{\overline{P}}{R_{air}T}, \; c = \sqrt{\gamma R_{air}T} \quad (4.7a, b)$$

Equation 4.8 represents the acoustic intensity (I) and acoustic power (P) for a simple plane wave with no reflection at a specific frequency. Substituting the expressions from Equation 4.7, it is seen that the acoustic intensity increases with the square root of the temperature. Therefore, the intensity levels should increase proportionally to increases in temperatures. This increase is not as obvious to show with the forward and reverse traveling waves found in the test rig, but a similar increase in the acoustic intensity can still be expected. Figure 4.29 shows how the intensity level increases in the combustor section when the temperature is increased from the ambient temperature to the operating temperature. On average, there is an increase of 8-10 dB in the acoustic intensity level in the bandwidth of interest. This is the maximum increase which would be expected since the combustor section has the highest operating temperature of any component of the test rig.

$$p = Ae^{j(\omega t - kx)}$$

$$I = \langle p\,u \rangle_T = \frac{|p^2|}{\rho c} = \frac{A^2}{\rho c} = \frac{A^2\sqrt{R_{air}T}}{\overline{P}\sqrt{\gamma}} \quad (4.8)$$

$$\mathrm{P} = IS$$

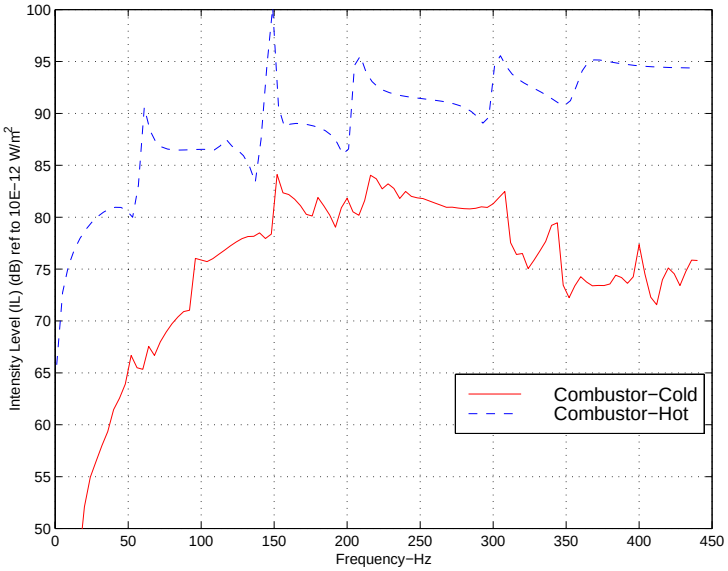

Figure 4.29-Comparison of acoustic intensity level for cold versus hot acoustics.

4.6.1-Temperature Profile in Test Rig

The elements in a 1-D transmission line acoustic model are well suited for applying a temperature profile to the test rig. Each element can have its own temperature thus allowing for temperature gradients in the model. The only restriction is that the temperature must be uniform at a given cross-section since the modeling technique can only capture 1-D effects. Figure 4.30 shows how the rig was subdivided into elements and Table 4.3 shows the specific temperatures used for each element.

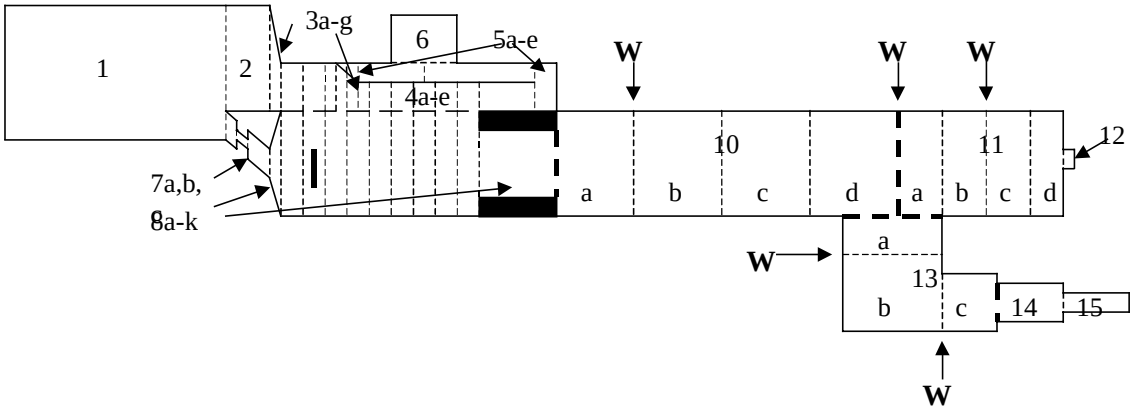

Figure 4.30-Full rig element model for temperature scaling.

Section	Temp (K)	Section	Temp (K)	Section	Temp (K)
		linear exit profile		parabolic exit profile	
1-3	600	10a	1160	10a	1114
4	700	10b	1080	10b	969
5-6	600	10c	1000	10c	848
7a	600	10d	920	10d	751
7b	800	11a	840	11a	685
7c	1000	11b	760	11b	637
8a	1840	11c	680	11c	610
8b	1800	11d	600	11d	600
8c	1740	12	600	12	600
8d	1680	13a	763	13a	663
8e	1620	13b	606	13b	590
8f	1560	13c	450	13c	529
8g	1500	14	425	14	452
8h	1440	15	400	15	400
8i	1380				
8j	1320				
8k	1240				

Table 4.3-Table of temperatures used in full rig element model.

The actual temperature values were estimated based on thermocouple measurements, theoretical flame temperature values, and assumptions. From measurements and theoretical values the temperature is known fairly accurately to the combustor exit. In the exhaust section though, no temperature data is available until the back-pressure valve (section 15), and the hot combustion gases are cooled in this section by a water spray. With known temperatures on each end of the region, different temperature profiles were used to analyze the sensitivity of the acoustic response to changing exhaust section temperatures. Figures 4.31a, b show that the difference between a linear and parabolic temperature profile is very small. Without experimental temperatures, it is not known if the temperature distribution fits either of these profiles. Due to the water spray, many other temperature profiles are possible including profiles such as step changes at each spray section.

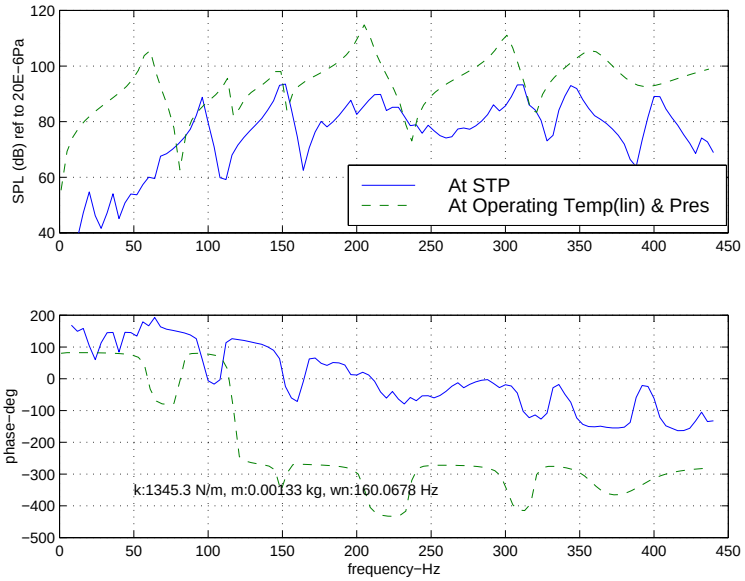

(a)

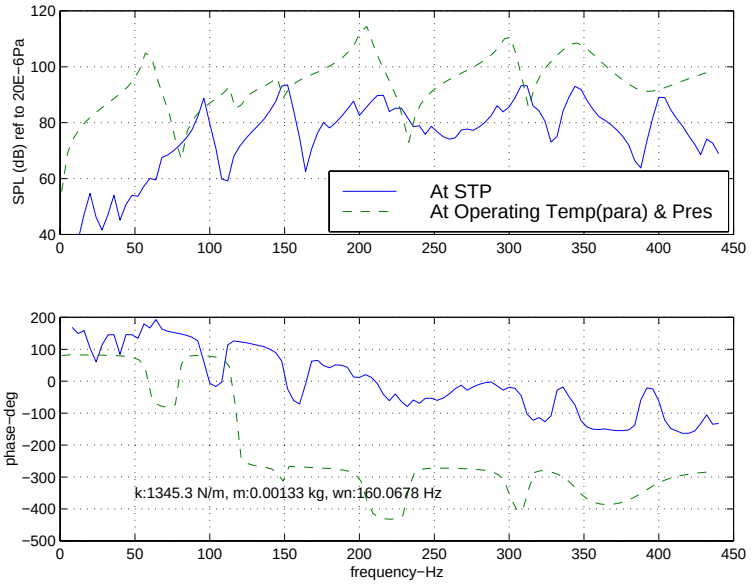

(b)

Figure 4.31a, b-FRF comparison of entire test rig at STP and at operating conditions: (a) Linear exit temperature profile. (b) Parabolic exit temperature profile.

From the cold acoustic modeling it is known that the fundamental model accurately captures the physical acoustic dynamics, but when the model acoustics are scaled to operating conditions, no experimental data exists to validate the model.

Obtaining experimental data for the hot acoustics is much more challenging and will be a topic for future work. Another condition which is hard to quantify is the affect of the water spray on the acoustics. Because water has a higher density and wave speed, the characteristic impedance of the spray will increase the impedance in the exit section of the test rig. Quantifying the additional impedance is challenging since the water is also being converted into water vapor as it encounters the hot exhaust gases. With no quantitative information available it was decided to not add any additional impedance. Understanding how acoustic waves are affected by a two phase water vapor is another topic for future work.

With the acoustic modeling complete the rest of the system must be modeled. This includes generating an unsteady heat release model and also a time delay element. Once these models have been created they can be assembled and used for a system stability analysis.